

## Analysis of Cardiac Myocyte Maturation Using CASA AV, a Platform for Rapid Dissection of Cardiac Myocyte Gene Function In Vivo

Yuxuan Guo,\* Nathan J. VanDusen,\* Lina Zhang, Weiliang Gu, Isha Sethi, Silvia Guatimosim, Qing Ma, Blake D. Jardin, Yulan Ai, Donghui Zhang, Biyi Chen, Ang Guo, Guo-Cheng Yuan, Long-Sheng Song, William T. Pu

**Rationale:** Loss-of-function studies in cardiac myocytes (CMs) are currently limited by the need for appropriate conditional knockout alleles. The factors that regulate CM maturation are poorly understood. Previous studies on CM maturation have been confounded by heart dysfunction caused by whole organ gene inactivation.

**Objective:** To develop a new technical platform to rapidly characterize cell-autonomous gene function in postnatal murine CMs and apply it to identify genes that regulate transverse tubules (T-tubules), a hallmark of mature CMs.

**Methods and Results:** We developed CRISPR/Cas9/AAV9-based somatic mutagenesis, a platform in which AAV9 delivers tandem guide RNAs targeting a gene of interest and cardiac troponin-T promoter-driven Cre to *Rosa<sup>Cas9GFP</sup>* neonatal mice. When directed against junctophilin-2 (*Jph2*), a gene previously implicated in T-tubule maturation, we achieved efficient, rapid, and CM-specific JPH2 depletion. High-dose AAV9 ablated JPH2 in 64% CMs and caused lethal heart failure, whereas low-dose AAV9 ablated JPH2 in 22% CMs and preserved normal heart function. In the context of preserved heart function, CMs lacking JPH2 developed T-tubules that were nearly morphologically normal, indicating that JPH2 does not have a major, cell-autonomous role in T-tubule maturation. However, in hearts with severe dysfunction, both adeno-associated virus-transduced and nontransduced CMs exhibited T-tubule disruption, which was more severe in the transduced subset. These data indicate that cardiac dysfunction disrupts T-tubule structure and that JPH2 protects T-tubules in this context. We then used CRISPR/Cas9/AAV9-based somatic mutagenesis to screen 8 additional genes for required, cell-autonomous roles in T-tubule formation. We identified RYR2 (Ryanodine Receptor-2) as a novel, cell-autonomously required T-tubule maturation factor.

**Conclusions:** CRISPR/Cas9/AAV9-based somatic mutagenesis is a powerful tool to study cell-autonomous gene functions. Genetic mosaics are invaluable to accurately define cell-autonomous gene function. JPH2 has a minor role in normal T-tubule maturation but is required to stabilize T-tubules in the failing heart. RYR2 is a novel T-tubule maturation factor. (*Circ Res.* 2017;120:1874-1888. DOI: 10.1161/CIRCRESAHA.116.310283.)

**Key Words:** alleles ■ gene silencing ■ heart failure ■ maturation ■ mutagenesis ■ transverse tubule

During mammalian heart development, cardiac myocyte (CM) phenotype changes dramatically between fetal, neonatal, and adult stages.<sup>1</sup> Fetal CMs are small, proliferative, and primarily produce energy through glycolysis. In contrast, adult CMs are much larger, terminally differentiated, and primarily produce energy through oxidative phosphorylation. The transition from fetal to adult phenotypes, referred to as CM maturation, occurs most rapidly in the perinatal period in the mouse between the end of gestation and about postnatal day 20 (P20). The

mechanisms that govern CM maturation are poorly understood. Presently, maturation of stem cells or nonmyocytes directed to differentiate into CMs is a major hurdle impeding the use of these technologies for disease modeling or therapeutic cardiac regeneration.<sup>1</sup> Understanding the factors that regulate endogenous CM maturation would facilitate efforts to overcome this hurdle.

**Editorial, see p 1846**  
**In This Issue, see p 1843**  
**Meet the First Author, see p 1844**

Original received November 10, 2016; revision received March 22, 2017; accepted March 29, 2017. In February 2016, the average time from submission to first decision for all original research papers submitted to *Circulation Research* was 15.4 days.

From the Cardiology, Boston Children's Hospital, MA (Y.G., N.J.V., Q.M., B.D.J., Y.A., D.Z., W.T.P.); Institute of Basic Medicine (L.Z.) and Pharmacology, School of Pharmacy (W.G.), Shanghai University of Traditional Chinese Medicine, China; Biostatistics and Computational Biology, Dana-Farber Cancer Institute, Boston, MA (I.S., G.-C.Y.); Physiology and Biophysics, Institute of Biological Sciences, Universidade Federal de Minas Gerais, Belo Horizonte, Brazil (S.G.); Cardiovascular Medicine, Department of Internal Medicine, François M. Abboud Cardiovascular Research Center, University of Iowa Carver College of Medicine, Iowa City (B.C., A.G., L.-S.S.); Veterans Affairs Medical Center, Iowa City (L.-S.S.); and Harvard Stem Cell Institute, Cambridge, MA (W.T.P.).

\*These authors contributed equally to this article.

The online-only Data Supplement is available with this article at <http://circres.ahajournals.org/lookup/suppl/doi:10.1161/CIRCRESAHA.116.310283/-/DC1>.

Correspondence to William T. Pu, MD, Department of Cardiology, Boston Children's Hospital, 300 Longwood Ave, Boston, MA 02115. E-mail [wpu@pubab.org](mailto:wpu@pubab.org)

© 2017 American Heart Association, Inc.

*Circulation Research* is available at <http://circres.ahajournals.org>

DOI: 10.1161/CIRCRESAHA.116.310283

## Novelty and Significance

### What Is Known?

- Genetic knockout or knockdown is a critical research strategy, but the commonly used approach requires developing and obtaining a different genetically modified mouse line for each gene, which is a slow process.
- Genetic knockout in the cardiac myocyte (CM) compartment often causes cardiac dysfunction, which initiates a panoply of secondary effects that can obscure the direct, cell-autonomous effects of gene inactivation.
- Junctophilin-2 is implicated in development of transverse tubules (T-tubules), a hallmark of CM maturation because knockdown of junctophilin-2 using shRNAs causes heart failure and T-tubule disruption.

### What New Information Does This Article Contribute?

- We developed a CM selective, Cas9/AAV9-mediated gene inactivation platform, named CRISPR/Cas9/AAV9-based somatic mutagenesis (CASA AV), that allows efficient inactivation of a gene without developing or acquiring a new mouse line for the gene of interest.
- On administration of different titers of adeno-associated virus constructs, both organ-wide and cell-autonomous effects of gene depletion can be studied, allowing dissection of direct cell-autonomous effects from the secondary effects because of cardiac dysfunction.

- Applying CASA AV approach to study T-tubule maturation, we found that junctophilin-2 plays a minor cell-autonomous role in T-tubule maturation, and we uncovered a novel, cell-autonomous role for RYR2 (Ryanodine Receptor-2) in T-tubule maturation.

CM-selective genetic loss of function is a powerful strategy for dissecting gene function in the heart. However, implementing this strategy using the traditional approaches is time-consuming, and results are vulnerable to misinterpretation because of secondary effects caused by organ-wide gene inactivation. Here, we show that a Cas9-based and adeno-associated virus-based platform (CASA AV) permits efficient and rapid gene inactivation, in either a small or large fraction of CMs. We deploy this new method to study T-tubule formation, a hallmark of mature CMs. Using the CASA AV platform, we show that junctophilin-2, a gene previously found to be essential for T-tubule maturation, has a limited role in this process. A CASA AV candidate-based screen uncovered an unanticipated role for RYR2 in T-tubule formation. The CASA AV platform and the mosaic gene inactivation strategy provide avenues to more rapidly and precisely perform *in vivo* genetic loss-of-function studies in CMs.

### Nonstandard Abbreviations and Acronyms

<b>AAV</b>	adeno-associated virus
<b>CASA AV</b>	CRISPR/Cas9/AAV9-based somatic mutagenesis
<b>CAV3</b>	caveolin-3
<b>CM</b>	cardiac myocyte
<b>cTNT</b>	cardiac troponin T promoter
<b>JPH2</b>	Junctophilin-2
<b>RYR2</b>	Ryanodine Receptor-2
<b>T-tubule</b>	transverse tubule

Among the most characteristic and latest developing hallmarks of adult CMs are transverse tubules (T-tubules), which start to form at  $\approx$ P10 in mouse and become fully mature at  $\approx$ P20.<sup>2</sup> T-tubules are tubular invaginations of the plasma membrane that penetrate deep within CMs and align with the Z-lines of sarcomeres. The junctional sarcoplasmic reticulum comes in close proximity to T-tubules at specialized membrane microdomains known as dyads, which mediate  $\text{Ca}^{2+}$ -induced  $\text{Ca}^{2+}$  release, and thereby couples CM electric activity to contraction. The cardiac action potential rapidly spreads along T-tubules, where depolarization activates the L-type  $\text{Ca}^{2+}$  channel. The resulting small influx of  $\text{Ca}^{2+}$  activates RYR2 (Ryanodine Receptor-2), the major cardiac intracellular  $\text{Ca}^{2+}$  release channel located on the junctional sarcoplasmic reticulum (SR). Activated RYR2 releases a large amount of  $\text{Ca}^{2+}$ , which induces sarcomere contraction. Thus, T-tubules facilitate coordinated  $\text{Ca}^{2+}$  release within large adult CMs which could not be achieved through sequential, diffusion-mediated spread of the  $\text{Ca}^{2+}$  transient.<sup>3,4</sup>

Although the physiological functions of T-tubules have been well characterized, the molecular machinery that induces the

maturation and maintenance of T-tubules is largely unknown. Junctophilin-2 (JPH2),<sup>5,6</sup> a structural protein that is specifically expressed in CMs, uses its N-terminal plasma membrane-binding motifs and C-terminal SR transmembrane domain to tether T-tubule and SR membrane together to form dyads.<sup>7</sup> CM-specific knockdown of *Jph2* in mouse caused dramatic remodeling and loss of T-tubules during postnatal development.<sup>2,8</sup> This result was interpreted as evidence that JPH2 is a critical regulator of T-tubule maturation.<sup>2,8</sup> However, JPH2 depletion in this mouse model also causes severe cardiomyopathy and heart failure.<sup>2,8</sup> T-tubule disruption is present in hearts with cardiomyopathy and heart failure.<sup>9,10</sup> Thus, cardiomyopathy and heart failure confound the interpretation of the *Jph2* knockdown phenotype with regard to its role in T-tubule maturation.

The confounding effect of secondary changes caused by cardiac stress response in conventional genetic analyses is a common problem for studies of CM maturation and indeed for cardiac biology in general. Genetic knockouts that induce cardiac dysfunction and failure precipitate a host of indirect secondary effects, and dissecting direct effects of genetic manipulations from secondary effects can be problematic. In this study, we established a platform for quickly producing genetic mosaic knockouts which allow investigation of cell-autonomous effects of gene knockout within the context of normally functioning myocardium. We deployed this platform to precisely characterize CM maturation factors without the interference of heart failure. We found that JPH2 is not required for overall T-tubule formation; rather, it helps to stabilize T-tubules in the face of cardiac dysfunction. We then use this platform and a candidate-based approach to identify novel T-tubule maturation factors. This platform will be useful for dissecting cell-autonomous genetic pathways that regulate postnatal CM maturation and function.

## Methods

Materials and Methods are available in the [Online Data Supplement](#).

### Adeno-Associated Virus

AAV-U6gRNA-cTNT-Cre plasmid (Online Figure I) was constructed by transferring a cTNT-Cre cassette from AAV-TNT-Cre plasmid<sup>11</sup> to PX552 plasmid.<sup>12</sup> A second U6gRNA was further added to generate AAV-U6gRNA<sub>1</sub>-U6gRNA<sub>2</sub>-cTNT-Cre (Addgene No. 87682). A total of 20 bp gRNA sequences (Online Table I) were cloned into these plasmids through a single ligation step.

Adeno-associated virus (AAV) was produced and purified using a standard protocol with modifications.<sup>13</sup> AAV titer was quantified by quantitative polymerase chain reaction using primers indicated in Online Table II.

### Mice

All animal procedures were approved by the Boston Children's Hospital Institutional Animal Care and Use Committee. AAVs were injected into P1 *Rosa<sup>Cas9GFP/Cas9GFP</sup>* mice<sup>14</sup> by subcutaneous injection. CMs were dissociated by retrograde collagenase perfusion as described previously.<sup>15</sup>

### Validation and Examination of *Jph2*

#### Depletion in CMs

The mRNA level of *Jph2* was examined by quantitative reverse transcription polymerase chain reaction (qRT-PCR) using primers shown in Online Table II. The deletion of *Jph2* between 2 gRNAs was detected by RT-PCR. Construction of DNA libraries for amplicon sequencing was performed by modifying a published protocol<sup>16</sup> using primers shown in Online Table II. Paired-end, 250 bp reads were generated on an Illumina MiSeq and analyzed using CRISPResso software.<sup>17</sup>

Validation of gene knockout was performed through immunofluorescence. Antibodies and dyes used are listed in Online Table III. Hearts were dissociated into single CMs through retrograde collagenase perfusion. Then, the CMs were briefly cultured to allow attachment to laminin-coated glass coverslips. Next, the CMs were fixed by 4% paraformaldehyde, and immunostaining was performed as described.<sup>18,19</sup> Confocal images were taken using Olympus FV1000 inverted laser scanning confocal microscope equipped with a 60X/1.3 silicone oil objective.

### Flow Cytometry

Quantitative analysis by flow cytometry was performed using a Propel Laboratories Avalon cytometer with a 100  $\mu$ m nozzle and standard GFP/RFP (green/red fluorescence protein) filter sets. Data were further analyzed using BioRad ProSort software.

Fluorescence-activated cell sorting was performed using a BD AriaII SORP cell sorter with a 100  $\mu$ m nozzle at Dana-Farber flow cytometry core facility.

### Analyses of Heart Phenotypes

Gross heart morphology was imaged under a stereomicroscope (Zeiss SteREO Discovery V8) with an AxioCam MRc camera. Heart histology, organ weights, and expression of cardiac stress markers were assayed as described previously.<sup>13</sup> Echocardiography was performed on awake animals using a VisualSonics Vevo 2100 with Vevostrain software. Echocardiography was performed blinded to AAV types and doses.

### T-Tubule Imaging and Analysis

In situ T-tubule imaging and AutoTT analysis of T-tubule patterns were performed as described previously.<sup>20</sup>

### Intracellular Ca<sup>2+</sup> Recording

Intracellular Ca<sup>2+</sup> was measured in isolated CMs that were loaded with Rhod-2 AM (acetoxymethyl). Cells were electrically stimulated at 1 Hz to produce steady-state conditions. All image data were acquired in the line scanning mode along the long axis of the cell using

an Olympus FV1000 inverted laser scanning confocal microscope with a 60X/1.3 silicone oil objective.

### Statistics

Unless otherwise noted, values are displayed as mean $\pm$ SD. Statistical comparisons were performed using Student *t* test. Kaplan–Meier survival analysis was performed using JMP software (SAS).

## Results

### CRISPR/Cas9/AAV9-Based Somatic Mutagenesis Efficiently Depletes *JPH2* in CMs During CM Maturation

Previously our laboratory showed that the heart could tolerate the deletion of essential genes in a small fraction of CMs while still maintaining normal heart function.<sup>11</sup> This mosaic analysis allowed us to study CM maturation in individual cells without the interference of secondary effects caused by heart failure. To establish a versatile technical platform that allows mosaic somatic mutagenesis of any gene specifically in CMs, we combined AAV-mediated mosaic transduction<sup>11</sup> with CRISPR/Cas9-based in vivo mutagenesis.<sup>14,21–24</sup> We constructed AAV vectors that contain 1 or 2 U6 promoter-driven gRNA expression cassettes and a cardiac troponin-T promoter that drives CM-specific expression of Cre recombinase (Figure 1A; Online Figure I). Using these vectors, we generated AAV9,<sup>25</sup> a cardiotropic AAV serotype, and subcutaneously injected the replication-deficient virus into *Rosa26<sup>Cas9-GFP</sup>* mice that harbor a Cre-inducible Cas9-P2A-GFP allele.<sup>14</sup> cTNT-Cre activated the expression of Cas9 and GFP specifically in AAV-transduced CMs, and the U6 promoter drove expression of gRNA(s) in these cells (Figure 1A). Thus, GFP<sup>+</sup> CMs express Cas9 nuclease activity that is directed specifically to target sites by gRNA(s). The nuclease creates DNA double-strand breaks at these target sites and triggers DNA damage repair by nonhomologous end joining, which is error prone and frequently results in insertions or deletions that can induce frameshift mutations silencing the targeted genes (Figure 1A).<sup>26</sup>

We first designed a gRNA that targets tdTomato gene and tested whether the tdTomato protein in *Rosa<sup>Cas9-GFP/tdTomato</sup>* mice is depleted by this CRISPR/Cas9/AAV9-based somatic mutagenesis (CASA9) system. We injected AAV-TNT-Cre (negative control) or AAV-gRNA(tdTomato)-TNT-Cre into P1 littermate pups and isolated CMs at 1 month by retrograde collagenase perfusion. The CMs were analyzed by flow cytometry to detect GFP and tdTomato. We found that tdTomato was depleted in  $\approx$ 89% GFP<sup>+</sup> CMs that were transduced by AAV expressing tdTomato gRNA (Figure 1B). No depletion was detected in GFP<sup>+</sup> CMs transduced with control AAV that lacked gRNA (Figure 1B; Online Figure II). Interestingly, although theoretically Cre should trigger expression of both Tomato and Cas9-P2A-GFP, we also detected tdTomato<sup>+</sup> GFP<sup>-</sup> cells (Online Figure II). Two effects likely resulted in these cells: (1) some CMs transiently harbor AAV, and limited Cre exposure activates tdTomato but not Cas9-P2A-GFP, as a result of differential sensitivity of these alleles to Cre activation and (2) GFP level was observed to be sensitive to CM stress, as occurs during CM dissociation and flow cytometry. The net effect is that a

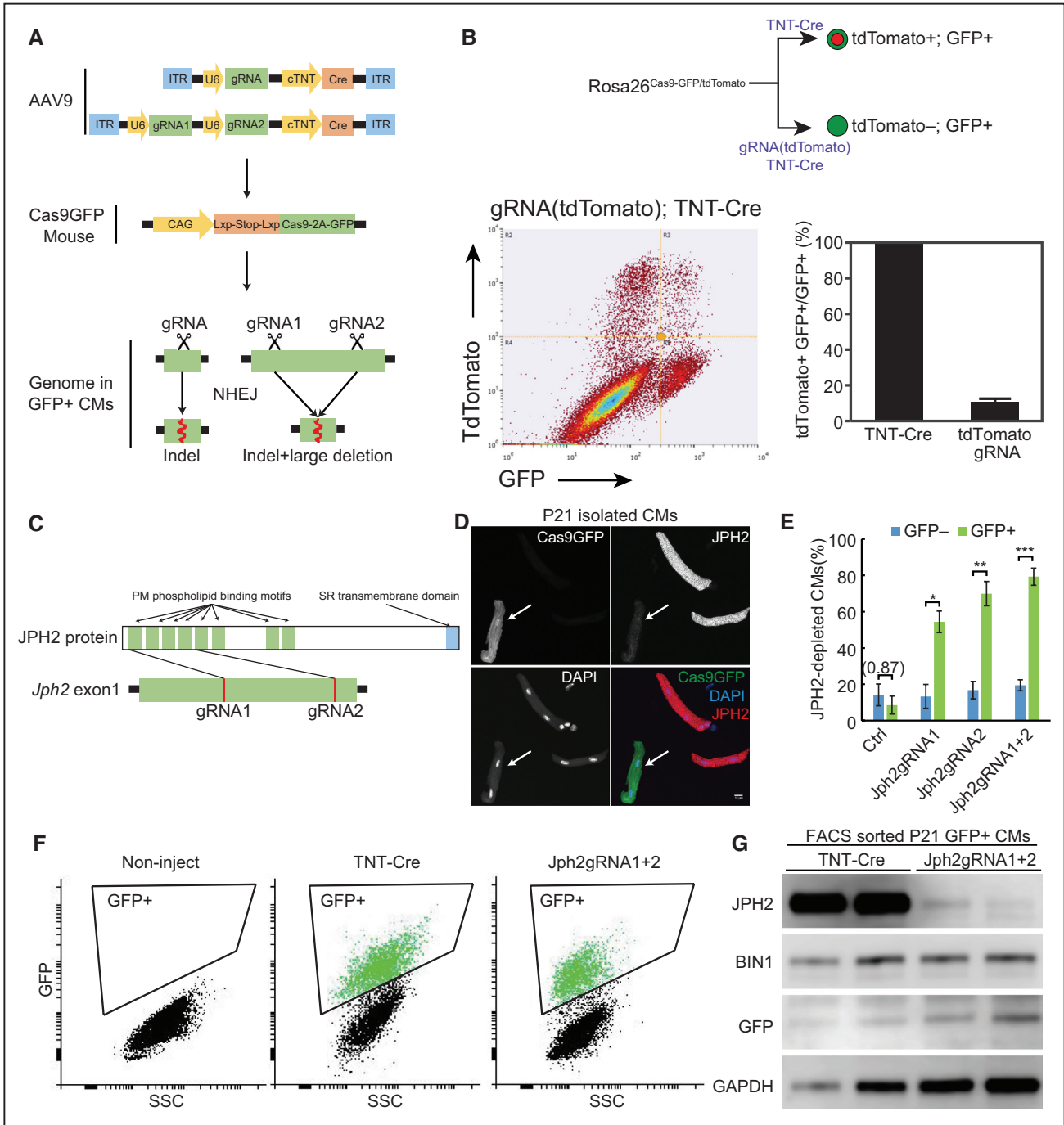


**Figure 1. CRISPR/Cas9/AAV9-based somatic mutagenesis (CASAAB) efficiently depleted *Jph2* in cardiac myocytes (CMs) during CM maturation in vivo.** **A**, Workflow for CASAAB. **B**, Depletion of tdTomato by AAV9 delivery of specific gRNA plus Cre to activate Cas9-P2A-GFP. Dot plot shows that most GFP<sup>+</sup> cells were tdTomato negative. As a control, AAV9 delivery of Cre without gRNA activated tdTomato in almost all GFP<sup>+</sup> cells (Online Figure II). **C**, Design of junctophilin-2 (*Jph2*) gRNAs that target the first coding exon of the *Jph2* gene. **D**, Immunostaining of JPH2 in isolated CMs demonstrated efficient depletion of JPH2 in Cas9GFP<sup>+</sup> CMs (arrow). Scale bar, 10  $\mu$ m. **E**, Quantification of the fraction of JPH2-depleted CMs among GFP<sup>-</sup> and GFP<sup>+</sup> CMs. More than 50 CMs were counted per heart. n=5 hearts. Student *t* test: \**P*<0.05; \*\**P*<0.01; \*\*\**P*<0.001. Nonsignificant *P* value is shown in parentheses. Plots show mean $\pm$ SD. **F** and **G**, Depletion of JPH2 in transduced (GFP<sup>+</sup>) CMs. Gating strategy for fluorescence-activated cell sorting (FACS) purification of isolated GFP<sup>+</sup> CMs is shown in **F**. **G**, Western blot analysis of FACS-sorted GFP<sup>+</sup> cells. SR indicates sarcoplasmic reticulum; and TNT, troponin-T.

minority of GFP<sup>-</sup> cells may have undergone Cas9 genome editing, a technical factor that needs to be considered when interpreting data (Discussion). Overall, this pilot experiment demonstrates that the CASAAB system mediates highly efficient gene silencing in CMs in vivo.

Next, we designed 2 gRNAs that target the coding sequence of *Jph2* within exon 1, which encodes the first 4 plasma membrane-binding motifs of JPH2 protein (Figure 1C). These gRNAs had at least 3 mismatches to any nontargeted sequences in the mouse reference genome (Online Figure

III A). We generated AAVs that expressed each gRNA individually (Jph2-gRNA1 or Jph2-gRNA2), or both simultaneously (Jph2-gRNA1+2), and injected  $1.1 \times 10^9$  vg/g (viral genomes per gram body weight) AAV into P1 *Rosa<sup>Cas9-GFP</sup>/<sup>Cas9-GFP</sup>* pups. We isolated CMs from P21 hearts and performed immunofluorescence to detect JPH2 protein (Figure 1D). We found that Jph2-gRNA1, Jph2-gRNA2, and Jph2-gRNA1+2 depleted JPH2 immunofluorescence in  $\approx 55\%$ ,  $\approx 70\%$ , and  $\approx 80\%$  of GFP<sup>+</sup> CMs, respectively (Figure 1E). We also analyzed JPH2 depletion in transduced CMs by using fluorescence-activated cell sorting to purify GFP<sup>+</sup> CMs, followed by Western blot (Figure 1F and 1G). Jph2-gRNA1+2 efficiently depleted JPH2 in transduced CMs. The level of BIN1, another protein implicated in T-tubule maturation,<sup>27</sup> was not affected (Figure 1G). The major effect of Jph2-gRNA1+2 was protein depletion rather than truncation (Online Figure IV), although we cannot exclude production of truncated protein in a low fraction of transduced cells. Overall, our data show that Jph2-CASA AAV efficiently depleted JPH2 in CMs and that 2 gRNAs were more efficient at achieving protein depletion than each single gRNA.

To determine the mechanisms that mediate this efficient JPH2 depletion, we injected  $5.5 \times 10^{10}$  vg/g AAV at P1, which is sufficient to transduce  $\approx 75\%$  CMs in the heart (Figure 2). At P7, we extracted RNA from heart apexes and detected significantly decreased *Jph2* mRNA after AAV-Jph2gRNA treatment by quantitative RT-PCR (Figure 3A and 3B). Analysis of *Jph2* transcript structure by RT-PCR demonstrated that dual-gRNA CASA AAV induced deletion of the intervening coding sequence between 2 gRNA targets in a subset of transcripts, which was not observed with either gRNA alone (Figure 3A and 3C). To more precisely define the effect of CASA AAV on *Jph2* transcripts, we amplified each gRNA-targeted site from cDNA and performed next-generation sequencing (Amplicon-Seq)<sup>28</sup> (Figures 2D through 2F and 3A; Online Figure IIIB and IIIC). Analysis of these sequences using CRISPResso<sup>17</sup> showed that gRNA1 alone generated mutations in 72% of transcripts, and 71% of these mutated reads shift the translational reading frame (Figure 3D). gRNA2 alone generated mutations in 61% of transcripts, and 86% of these mutated reads shift the translational reading frame (Figure 3D). These mutations localized to the expected gRNA cleavage sites (Figure 3E). When both gRNAs were present, frameshift mutations were detected in  $>80\%$  mutated reads, and these mutations occurred between the 2 gRNA-targeted sites (Figure 3D through 3F). Thus, JPH2 protein depletion induced by CASA AAV is because of a combination of frame-shifting mutations and mRNA decrease, potentially resulting from nonsense-mediated decay.<sup>29</sup> The use of 2 gRNAs increased the efficiency of both of these effects. Deletion of *Jph2* coding sequences that encode critical plasma membrane-binding domains between the 2 gRNA-targeted sites also provides potential mechanisms to perturb the stability and function of JPH2 protein (Figures 1C, 3C, and 3F).

### AAV-Mediated Mosaic Infection Avoids Cardiomyopathies Caused by JPH2 Depletion

To determine the effect of AAV dosage on whole organ and individual CM phenotypes, we treated mice with serial dilutions

of AAV-gRNA(Jph2)1+2-TNT-Cre, referred to subsequently as AAV-gRNA(Jph2), at P1. We defined the mice receiving  $1.1 \times 10^9$ ,  $6.1 \times 10^9$ ,  $1.8 \times 10^{10}$ , and  $5.5 \times 10^{10}$  vg/g AAV doses as Jph2\_Low, Jph2\_Mid, Jph2\_High, and Jph2\_Full groups, respectively. We measured the frequency of transduced CMs at P7 by detecting Cre-dependent GFP expression from the *Rosa26<sup>Cas9-GFP</sup>* allele. AAV dose was positively correlated to the myocardial area occupied by GFP<sup>+</sup> CMs (Figure 2A). We quantified the frequency of GFP<sup>+</sup> CMs in dissociated CM preparations. Jph2\_Low, Jph2\_Mid, Jph2\_High, and Jph2\_Full groups expressed GFP in 22%, 47%, 64%, and 75% of CMs, respectively (Figure 2B).

Next, we investigated whether AAV dosage influences the efficiency of JPH2 depletion in individual transduced CMs. We performed immunofluorescence staining of JPH2 in CMs that were treated with different AAV doses at P1 and isolated at P7. The control AAV-TNT-Cre virus (lacking gRNA) was administered at the full dose ( $5.5 \times 10^{10}$  vg/g). Immunostaining of JPH2 was used to measure each cell's JPH2 expression level, and immunostaining of caveolin-3 (CAV3), a plasma membrane marker, defined the boundary of each single cell (Figure 2C and 2D). We found a  $\approx 70\%$  decrease of JPH2 intensity in Jph2-CASA AAV-treated CMs when compared with negative controls, which further confirmed the efficient depletion of JPH2 protein. By immunostaining, there was no detectable difference in intensity between GFP<sup>+</sup> CMs that were treated with different doses of AAVs (Figure 2D). To examine the impact of AAV dosage on the efficiency of protein depletion, we performed fluorescence-activated cell sorting of GFP<sup>+</sup> cells in each group and analyzed JPH2 expression by Western blotting (Figure 2E). This demonstrated efficient JPH2 depletion in all groups, although the protein remained detectable in the Jph2\_Low and Jph2\_Mid groups but was undetectable in the Jph2\_High and Jph2\_Full groups. Thus, AAV dose primarily determines the frequency of transduced CMs. The dose has a small effect on protein depletion efficiency among transduced cells, but even at the lowest dose tested, the protein was efficiently depleted. These findings are important for interpreting the mosaic gene knockout data presented below.

Mice that received the full dose of AAV-gRNA(Jph2) died between P10 and P13 (Figure 4A), which is consistent with the survival curve of *Myh6-Cre;Jph2-shRNA* mice described previously.<sup>8</sup> Mice treated with the other doses of AAV-gRNA(Jph2) survived beyond P20 (Figure 4A), when T-tubules become fully mature.<sup>2</sup> Because our goal was to examine the impact of *Jph2* on T-tubule maturation, we focused the following studies on Jph2\_Low, Jph2\_Mid, and Jph2\_High groups and studied mice at P21 to P24. Analyses of gross heart morphology showed that Jph2\_High and Jph2\_Mid groups had cardiac hypertrophy and dilatation, which were not evident in the Jph2\_Low group (Figure 4B). This difference was quantified by measurement of the heart weight/body weight ratio, which was not elevated in the Jph2\_Low group but was increased in Jph2\_Mid and Jph2\_High groups in a dose-dependent manner (Figure 4C). Echocardiography showed severely depressed heart systolic function in the Jph2\_High group (Figure 4D). By contrast, the Jph2\_Mid group had moderately depressed heart function, and the

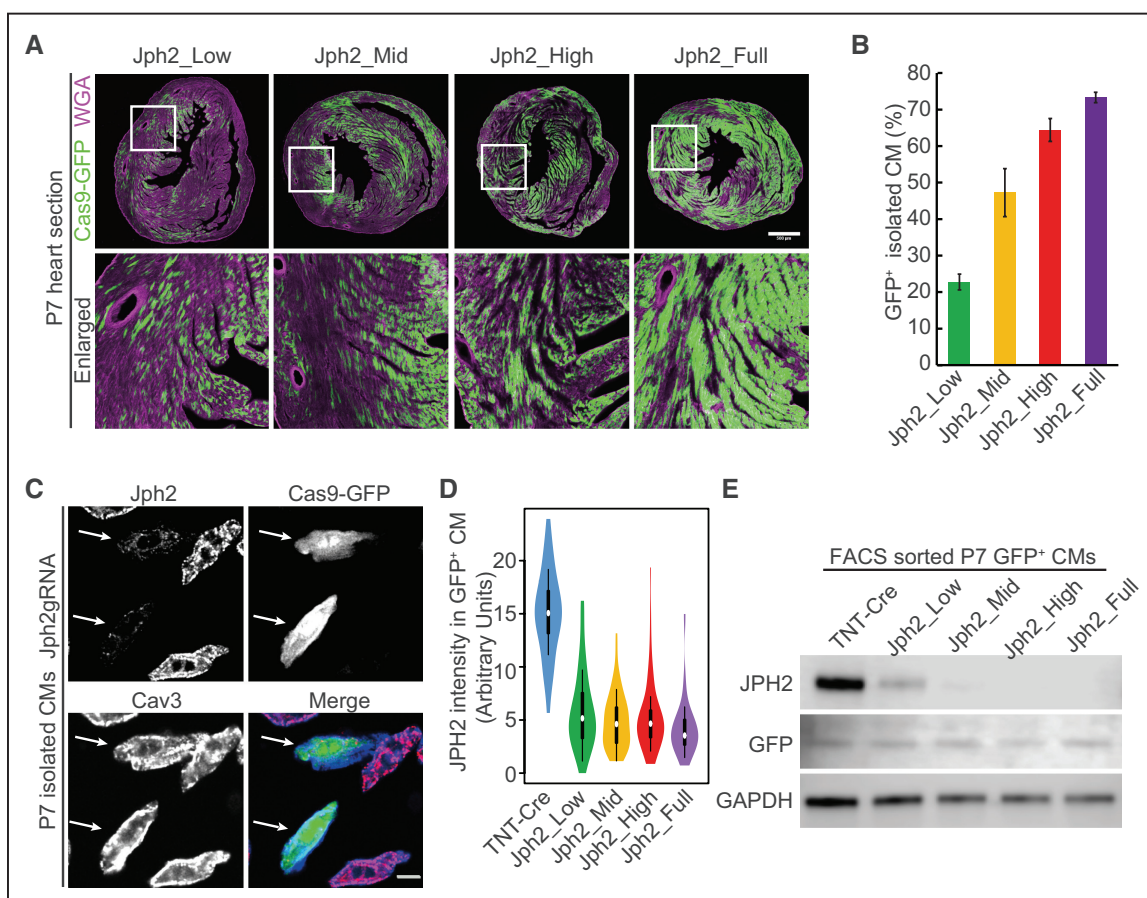


**Figure 2. Effect of adeno-associated virus (AAV) dosage on the frequency of cardiac myocyte transduction and the extent of Junctophilin-2 (JPH2) depletion.** **A**, Representative images of GFP<sup>+</sup> cardiac myocytes (CMs) in postnatal day 7 (P7) heart sections that were infected with different doses of AAVs. Scale bar, 500  $\mu$ m. Boxed area were enlarged at **bottom**. **B**, Quantification of the fraction of GFP<sup>+</sup> CMs that were isolated from P7 hearts infected with different doses of AAVs. n=3 hearts. More than 400 CMs were counted per heart. **C**, Immunostaining of JPH2 in CMs isolated from P7 hearts. Arrows point to GFP<sup>+</sup> CMs that were depleted of JPH2. Scale bar, 10  $\mu$ m. **D**, Violin plots of JPH2 immunofluorescence intensity in maximally projected confocal images of P7 CMs. For each group, n=60 CMs isolated from 3 hearts. White circles and boxes indicate medians and 25th and 75th percentiles. Whiskers extend 1.5 $\times$  the interquartile range from the 25th to 75th percentiles. Colored shapes show density estimates of the data. **E**, Immunoblot showing level of JPH2 protein in GFP<sup>+</sup> CMs from the indicated treatment groups. TNT indicates troponin-T.

Jph2\_Low group did not exhibit detectable heart dysfunction (Figure 4D). AAV-gRNA(Jph2) dosage also correlated with the extent of left ventricular dilatation (Figure 4E and 4F). Expression of cardiac stress markers *Myh7*, *Nppa*, and *Nppb* were consistent with these overall effects of virus dose on heart structure and functions (Figure 4G). Together, these data indicate that high and mid doses of AAV-gRNA(Jph2) caused dose-related cardiac hypertrophy and dysfunction, as previously reported in *Jph2* shRNA genetic mouse models,<sup>2,8</sup> whereas the low dose did not impact heart function at the organ level.

We next examined the effect of the extent of *Jph2* inactivation on the responses of individual CMs. Although induction of heart dysfunction correlated with increased CM size, there was no difference in CM size between GFP<sup>+</sup> and GFP<sup>-</sup> CMs at any viral dose (Figure 4H). Thus, JPH2 depletion does not directly affect CM size. Rather, JPH2 affects CM size indirectly through effects on overall organ function.

Collectively, these data show that a low dose of AAV-gRNA(Jph2) can be used to achieve mosaic depletion of JPH2 without affecting overall organ function. Mid and high doses

increase the fraction of CMs with gene inactivation and correspondingly cause organ dysfunction and global stress responses.

### JPH2 Plays a Minor Role in T-Tubule Maturation

Because mosaic *Jph2* inactivation by low-dose AAV-gRNA(Jph2) avoided secondary effects of organ dysfunction, we were able to precisely examine the role of JPH2 in T-tubule organization without the confounding effects of cardiac dysfunction. To observe T-tubule organization in live CMs in intact heart ventricles, we labeled T-tubules with the plasma membrane dye FM 4-64 through retrograde heart perfusion and performed in situ confocal imaging.<sup>2,30</sup> We found that T-tubules were dramatically disrupted in GFP<sup>+</sup> CMs in Jph2\_High mice. However, this phenotype was mild in GFP<sup>+</sup> CMs in Jph2\_Mid mice. No overt disruption in T-tubules was observed in GFP<sup>+</sup> CMs in Jph2\_Low mice (Figure 5A and 5B; see additional representative confocal z stacks in Online Movies I through III). We analyzed the changes in T-tubules in details by performing unbiased quantification of T-tubule morphology using AutoTT software<sup>20</sup> (Figure 5B). This software objectively quantifies transverse T-tubule elements,

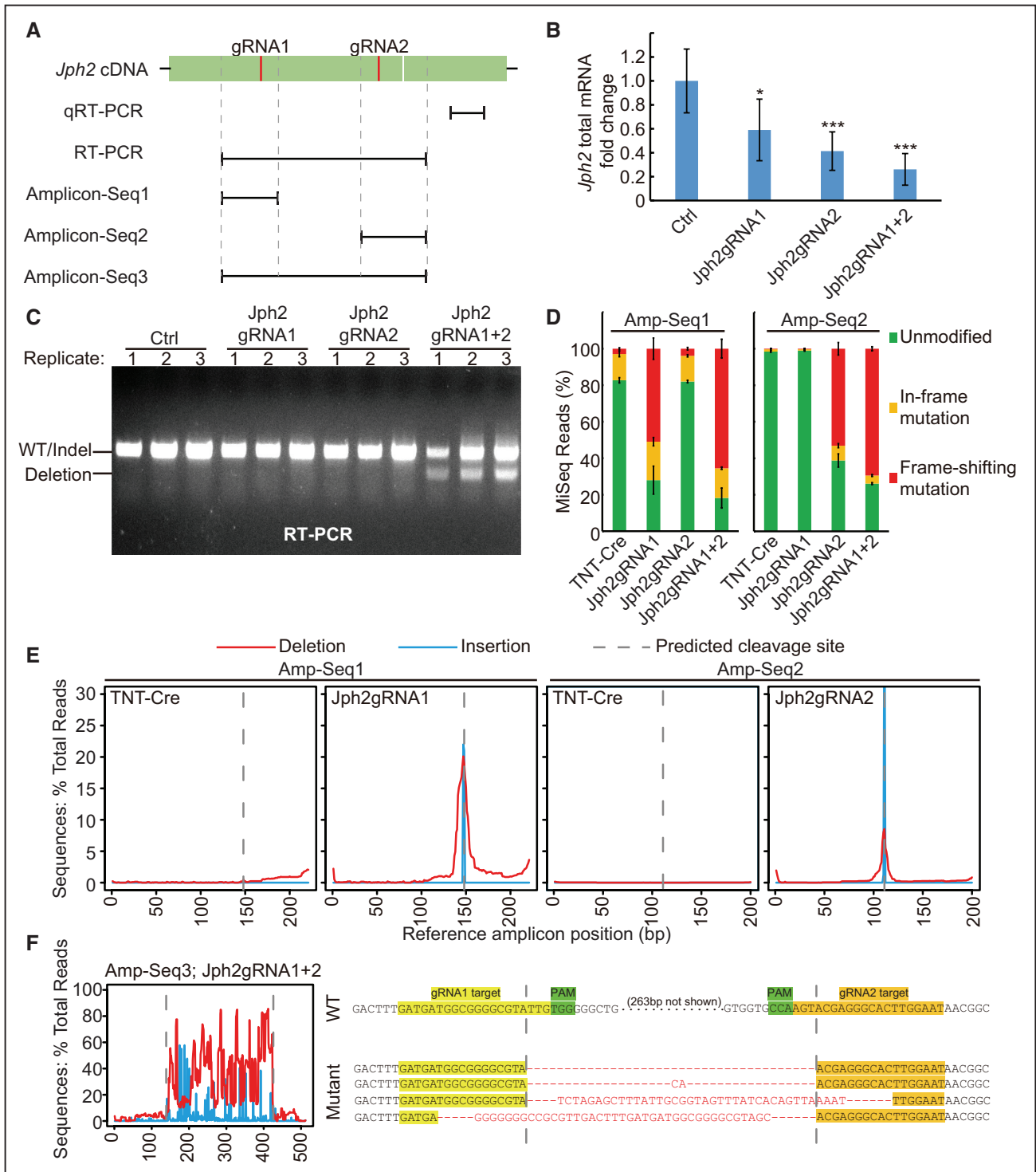


**Figure 3. Multiple mechanisms mediate efficient *Jph2* depletion in cardiac myocytes (CMs).** **A**, A scheme of targeted loci on *Jph2* cDNA for qRT-PCR, RT-PCR and Amplicon-Seq analyses. **B**, qRT-PCR analysis of *Jph2* mRNA level. n=6 postnatal day 7 (P7) heart apexes. Student *t* test: \**P*<0.05; \*\**P*<0.01; \*\*\**P*<0.001. **C**, Expression of tandem gRNAs induced deletion between the gRNAs. Transcript structure was interrogated by RT-PCR. **D**, Quantification of in-frame and frame-shifting mutations identified by Amplicon-Seq. n=3 biological replicates. A total of 300 to 2000 reads were analyzed per sample. **E**, Distribution of small insertions and deletions along cDNA amplicon 1 and 2. **F**, Analysis of mutation distribution in Amplicon 3 (left) reveals large deletions between gRNA1 and 2 target sites. Representative sequencing results in amplicon 3 are shown (right). Deleted or unaligned sequences are in red. Plots show mean±SD in (B) and (D). *Jph2* indicates junctophilin-2; and TNT, troponin-T.

longitudinal T-tubule elements, total T-tubule elements (which equal to transverse T-tubule elements+longitudinal T-tubule elements), and T-tubule regularity.<sup>20</sup> Compared with

GFP<sup>-</sup> internal control CMs, GFP<sup>+</sup> CMs in *Jph2*\_Low group showed no significant change in T-tubule regularity or longitudinal T-tubule elements and subtly but significantly reduced

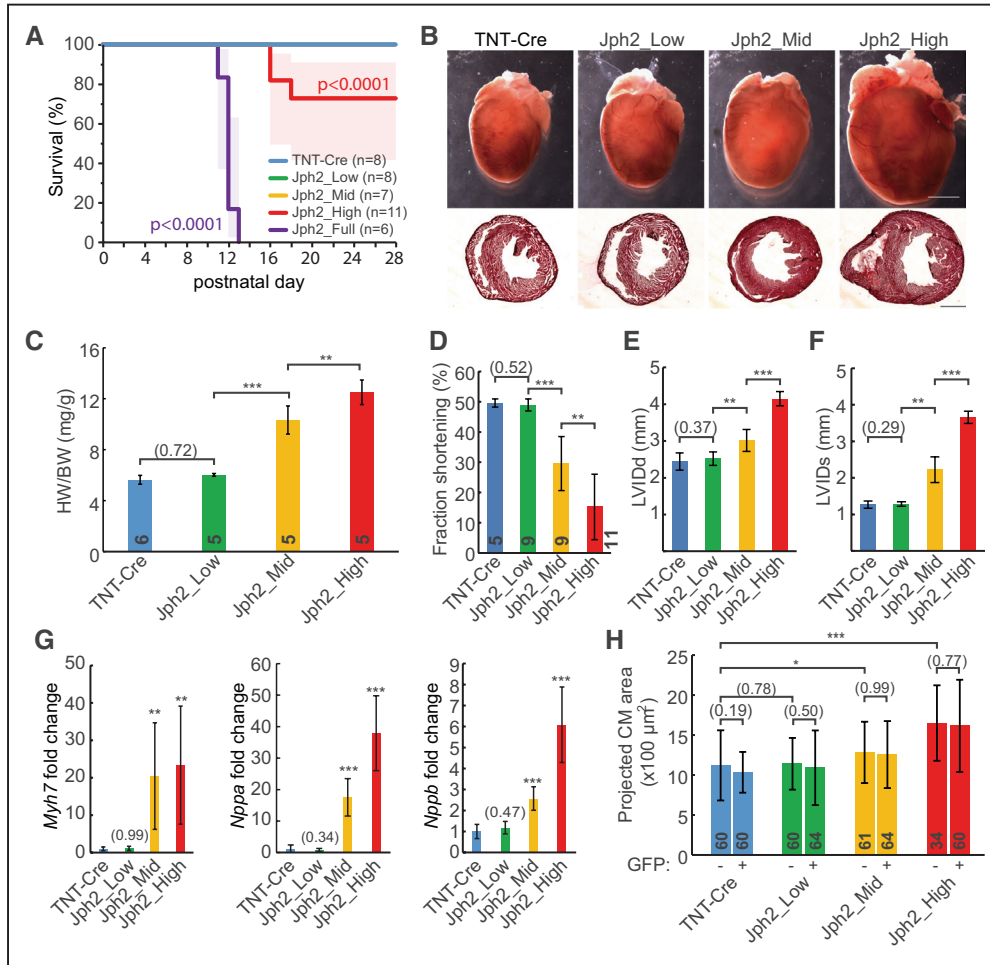


**Figure 4. Dose-dependent induction of myocardial dysfunction by AAV-gRNA(Jph2).** **A**, Kaplan–Meier analysis of survival curve under control or different doses of Jph2gRNA adeno-associated virus (AAV) treatments. **B**, Representative whole-heart brightfield images (**above**) and Hematoxylin and Eosin–stained frozen cross sections (**bottom**). Scale bar, 2 mm. **C**, Heart weight (HW):body weight (BW) ratio at P21. **D–F**, Echocardiographic analysis of heart size and function in P21 mice treated with indicated doses of Jph2gRNA AAV. **G**, qRT-PCR measurement of heart stress markers. mRNA extracted from P21 to P24 heart apexes were analyzed. n=6 hearts. **H**, Cell size analysis of isolated cardiac myocytes (CMs). CMs were isolated from 3 hearts in each group. Student *t* test: \**P*<0.05; \*\**P*<0.01; \*\*\**P*<0.001. Nonsignificant *P* values are shown in parentheses. Numbers in bars indicate sample size. Plots show mean±SD. Jph2 indicates junctophilin-2; LVIDd, left ventricular internal diameter end diastole; LVIDs, left ventricular internal diameter end systole; and TNT, troponin-T.

transverse T-tubule elements and total T-tubule elements (Figure 5C through 5F). The Jph2\_Mid group also showed no significant change in longitudinal T-tubule elements, but a significant impairment in the other 3 parameters was greater than in the Jph2\_Low group. All of these parameters were most dramatically impaired in the Jph2\_High group. T-tubules in GFP<sup>-</sup> CMs from Jph2\_High mice exhibited T-tubule defects, which were more severe than GFP<sup>+</sup> CMs in Jph2\_Low and Jph2\_Mid mice. These data are consistent with previous observations that T-tubules remodel and become disorganized in wild-type CMs in pathological conditions.<sup>9</sup> The GFP<sup>+</sup> CMs in Jph2\_High mice had substantially more disrupted T-tubules than their GFP<sup>-</sup> counterparts (Figure 5C through 5F), suggesting a cell-autonomous role for JPH2 to protect T-tubules from remodeling in heart failure.<sup>31</sup> We also examined the effect of JPH2 depletion on sarcomere structure, as assessed by immunostaining for Z-line marker sarcomeric  $\alpha$ -actinin (Actn2; Online Figure V). Z-line spacing and regularity, measured by AutoTT,<sup>20</sup> were not significantly affected by JPH2 depletion

(Online Figure V). Together these data demonstrate that JPH2 has a minor cell-autonomous function in T-tubule organization that is exacerbated by heart failure.

To further confirm that these varied phenotypes were not caused by JPH2 depletion efficiency, we performed dual-color immunofluorescence to detect both JPH2 and CAV3 in CMs dissociated from AAV-TNT-Cre (control)–treated and AAV-gRNA(Jph2)–treated mice. This permitted us to identify true JPH2-deficient CMs and examine CAV3 pattern in these CMs (Figure 6A). Consistent with in situ T-tubule imaging results, JPH2<sup>-</sup> CMs that were derived from Jph2\_Low mice exhibited normal global T-tubule morphology when compared with JPH2<sup>+</sup> control CMs (Figure 6A). By contrast, Jph2\_Mid and Jph2\_High mice exhibited disrupted CAV3 patterns in JPH2<sup>-</sup> CMs (Figure 6A). AutoTT quantification of CAV3 immunostaining also showed significantly decreased total T-tubule elements and regularity in JPH2<sup>-</sup> CMs isolated from Jph2\_Mid and Jph2\_High mice, but no statistically significant difference between Jph2\_Low and control was observed (Figure 6B and

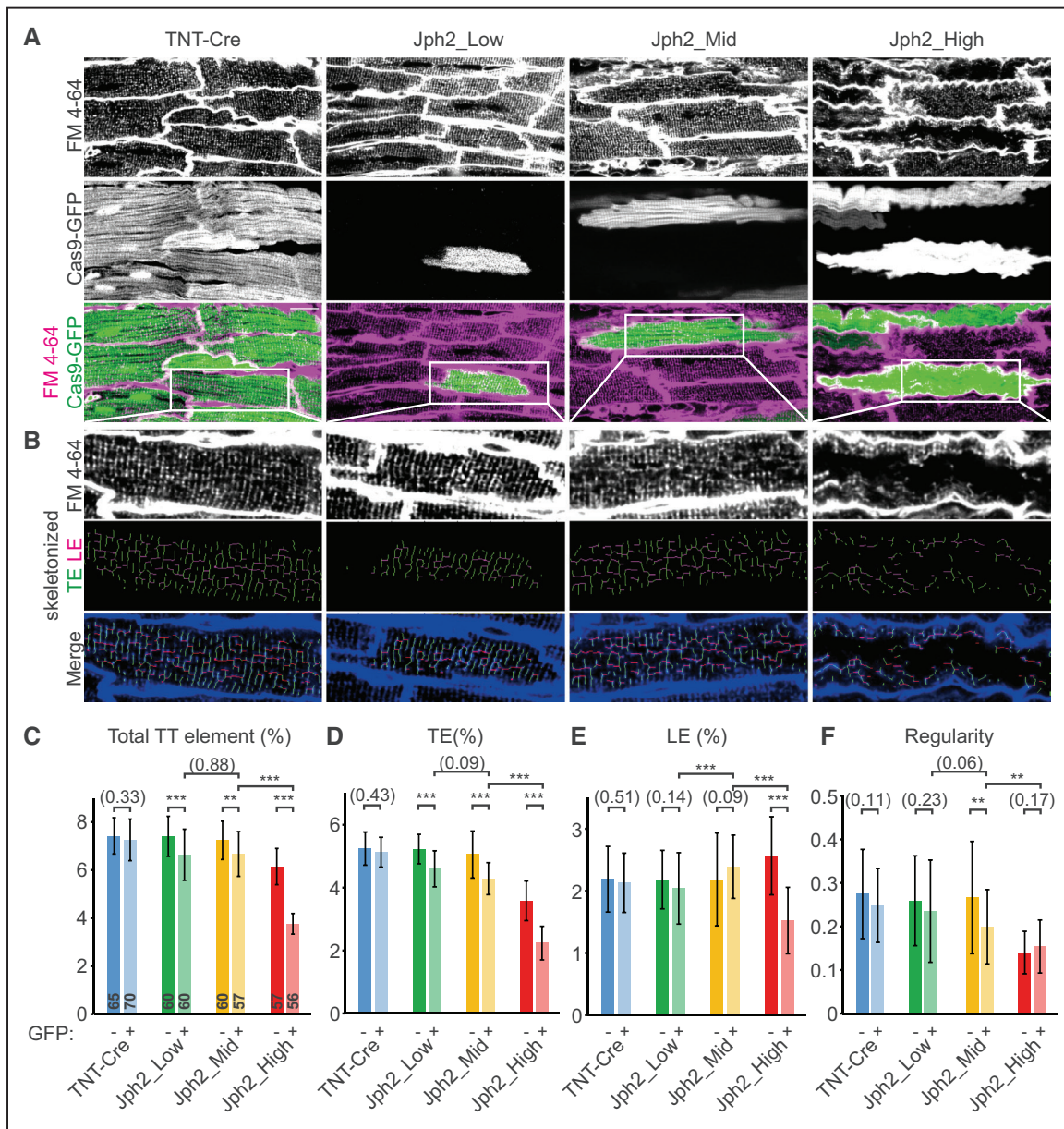


**Figure 5. In situ transverse tubule (T-tubule) analysis of cardiac myocytes with mosaic junctophilin-2 (JPH2) depletion.** **A**, In situ confocal live imaging of T-tubules in FM4-64-loaded postnatal day 21 (P21) hearts under control or mosaic JPH2 depletion. Scale bar, 20  $\mu$ m. **B**, T-tubule patterns in white boxes in **(A)** were enlarged and skeletonized. **C-F**, AutoTT quantification of T-tubule patterns under in situ imaging. Number of CMs analyzed is shown in columns in **(C)**. CMs were dissociated from 3 hearts. Student *t* test: \*\**P*<0.01; \*\*\**P*<0.001. Nonsignificant *P* values are shown in parentheses. Plots show mean $\pm$ SD. LE indicates longitudinal element; TE, transverse element; Total TT element=TE+LE; and TNT, troponin-T.

6C). It is possible that this experiment did not reproduce the mild T-tubule defects in Jph2\_Low that were observed by in situ T-tubule imaging (Figure 5) because the CM dissociation procedure affects T-tubule organization in some CMs and thereby increases within-group variation (compare error bars between Figure 5 and Figure 6). However, based on both in situ T-tubule analysis and CAV3 analysis on isolated CMs, it is clear that JPH2 has a minor direct function in T-tubule maturation. Substantial T-tubule disruption was only observed when JPH2 was depleted in a large fraction of CMs, resulting in cardiac stress and associated secondary effects on CMs (Figure 6D).

We next evaluated whether the varied effect of JPH2 depletion on T-tubule organization influences Ca<sup>2+</sup> handling.

Freshly dissociated CMs were loaded with the Ca<sup>2+</sup>-sensitive dye Rhod-2 AM, and Ca<sup>2+</sup> transients were measured by confocal line scan imaging. Both transduced and nontransduced Jph2\_High CMs exhibited significantly reduced Ca<sup>2+</sup> transient amplitude, prolonged time to peak, and slower time to 50% decay (Figure 7A and 7B), which is consistent with previous studies of JPH2's role in Ca<sup>2+</sup> handling.<sup>2</sup> However, the major effect was likely secondary to heart failure and not directly attributable to JPH2 depletion because the difference with TNT-Cre control and Jph2\_High CMs was greater than the difference between GFP<sup>+</sup> and GFP<sup>-</sup> CMs within Jph2\_High. Ca<sup>2+</sup> transient amplitude was more severely depressed in GFP<sup>+</sup> than GFP<sup>-</sup> Jph2\_High CMs, consistent with

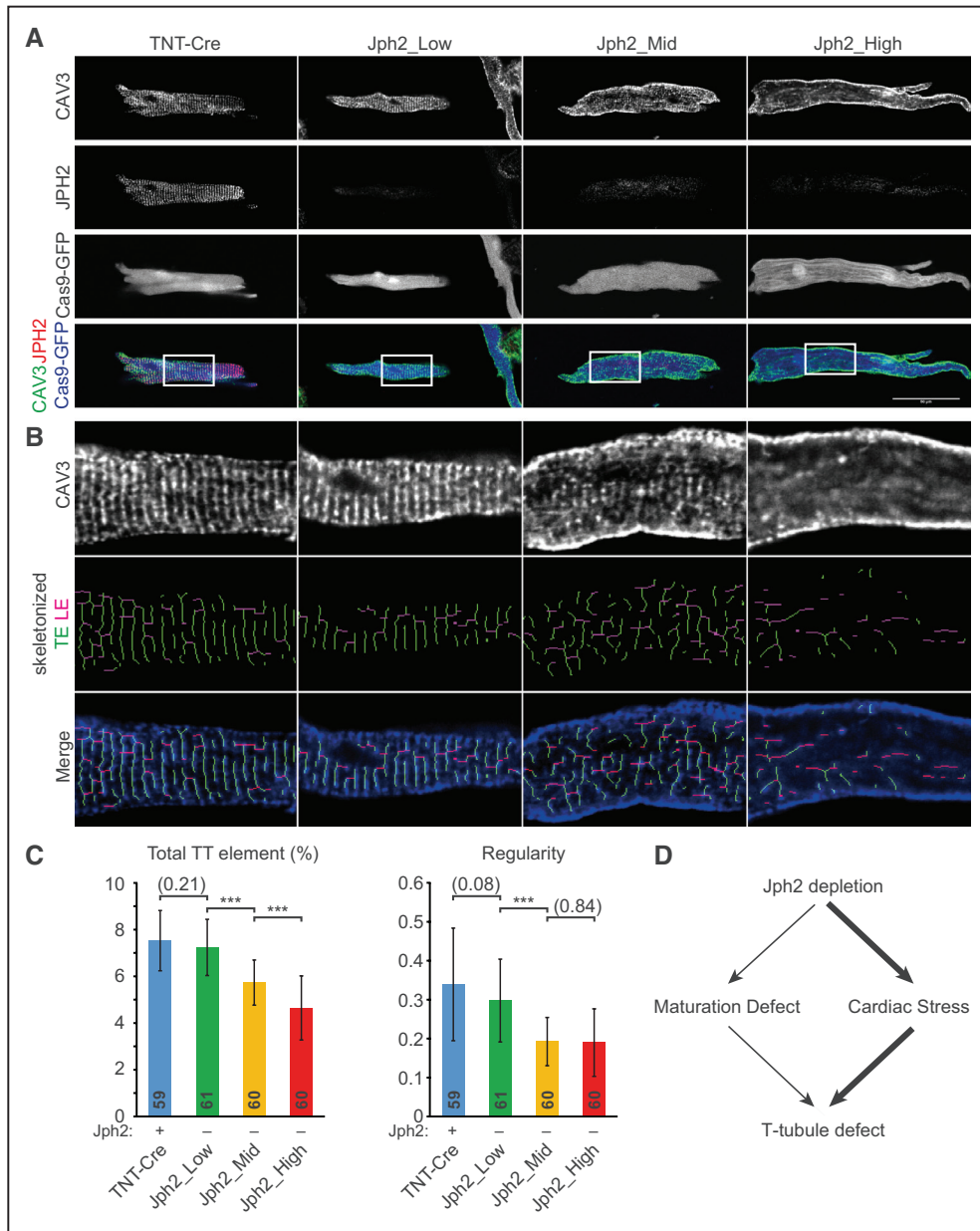


**Figure 6. Transverse tubule (T-tubule) analysis in cardiac myocytes (CMs) that were isolated from hearts under serial levels of mosaic junctophilin-2 (JPH2) depletion.** **A**, Representative images of CAV3 and JPH2 staining in CMs isolated from postnatal day (P21) hearts under control or different levels of mosaic JPH2 depletion. Scale bar, 50  $\mu$ m. CAV3 patterns in white boxes were enlarged and skeletonized in **(B)**. **C**, AutoTT quantification of T-tubule patterns in isolated CMs. Number of CMs analyzed was shown in columns in **(C)**. CMs were dissociated from 3 hearts per group. Student *t* test: \*\**P*<0.01; \*\*\**P*<0.001. Nonsignificant *P* values are shown in parentheses. Plots show mean $\pm$ SD. **D**, JPH2 depletion had a small cell-autonomous effect of T-tubule structure. Depletion in a large fraction of cardiac myocytes caused heart failure, which indirectly disrupted T-tubule structure. TNT indicates troponin-T.

the more severe T-tubule abnormalities observed in GFP<sup>+</sup> versus GFP<sup>-</sup> Jph2\_High CMs. Jph2\_Low GFP<sup>+</sup> CMs had Ca<sup>2+</sup> transients with mildly but significantly reduced peak amplitude compared with GFP<sup>-</sup> CMs isolated from the same heart. No significant change in time to peak or time to 50% decay was detected (Figure 7C and 7D). This is consistent with the minor effect of JPH2 depletion on T-tubule morphology in Jph2\_Low. These single-cell measurements of Ca<sup>2+</sup> handling paralleled our imaging data on T-tubule structure and indicate that JPH2 has a minor cell-autonomous role in establishing Ca<sup>2+</sup> release unit function.

### CASA AV-Based Screen Identifies RYR2 as a Novel T-Tubule Regulator

Mosaic mutagenesis by CASA AV avoids the time-consuming procedure of generating genetically modified mice. A large number of AAVs that deliver gRNAs directed at different genes can be generated side by side simultaneously. Thus, this technology allowed us to perform a genetic screen for novel T-tubule regulators. Using a candidate-based approach, we generated AAVs targeting 8 genes that could be potentially important for T-tubule maturation. These genes encode important cardiac transcriptional factors (NKX2-5

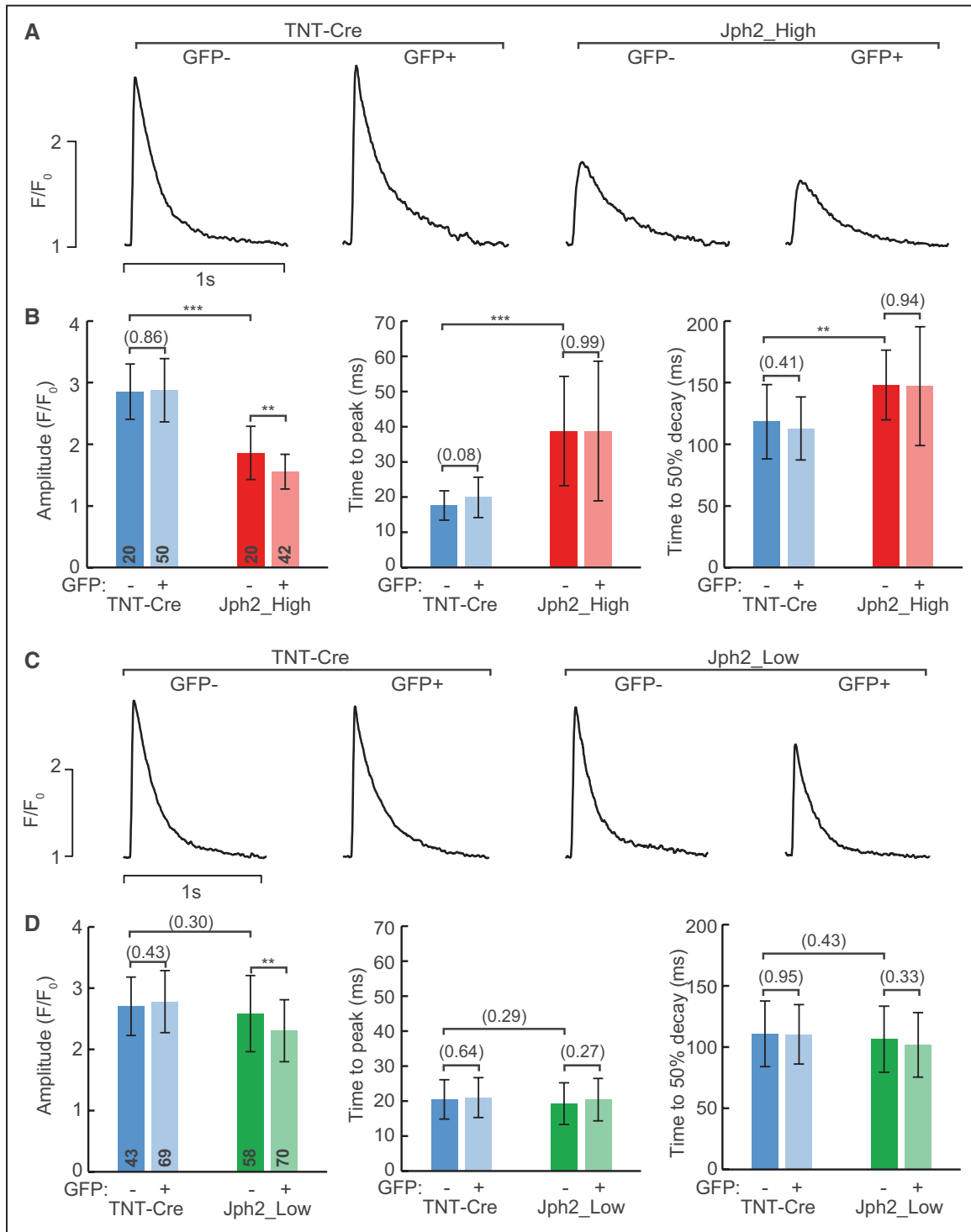


**Figure 7. Effect of junctophilin-2 (JPH2) depletion on Ca<sup>2+</sup> transients in ventricular cardiac myocytes (CMs).** CMs were dissociated from control, Jph2\_High (A and B), or Jph2\_Low (C and D) treatment groups. CMs were loaded with the Ca<sup>2+</sup>-sensitive dye Rhod-2 AM (acetoxymethyl) and imaged by confocal line scan. Representative Ca<sup>2+</sup> transient profiles recorded from cardiac myocytes paced at 1 Hz are shown in A and C, and quantitative data are shown in B and D, plotted as mean±SD. Number within bars indicates the number of CMs whose data were pooled to calculate the bar. These CMs were isolated from 3 hearts per group. Groups were compared by *t* test. \*\**P*<0.01. \*\*\**P*<0.001. Nonsignificant *P* values are shown in parentheses. TNT indicates troponin-T.

[NK2 homeobox 5], TBX5 [T-box 5], MEF2C [myocyte enhancer factor 2C], and TEAD1 [TEA domain family member 1]) and T-tubule-associated proteins (RYR2, CACNA1C [calcium voltage-gated channel subunit alpha1 C], CAV3, and NCX1 [sodium-calcium exchanger 1]). We injected

each of these viruses into P1 Rosa26<sup>Cas9-P2A-GFP</sup> mice at a low dose (similar to that used in Jph2\_Low), dissociated the hearts at P21, and performed JPH2 immunostaining to image T-tubule morphology in GFP<sup>+</sup> CMs (Figure 8A). GFP<sup>+</sup> CMs from the same heart were used as internal negative

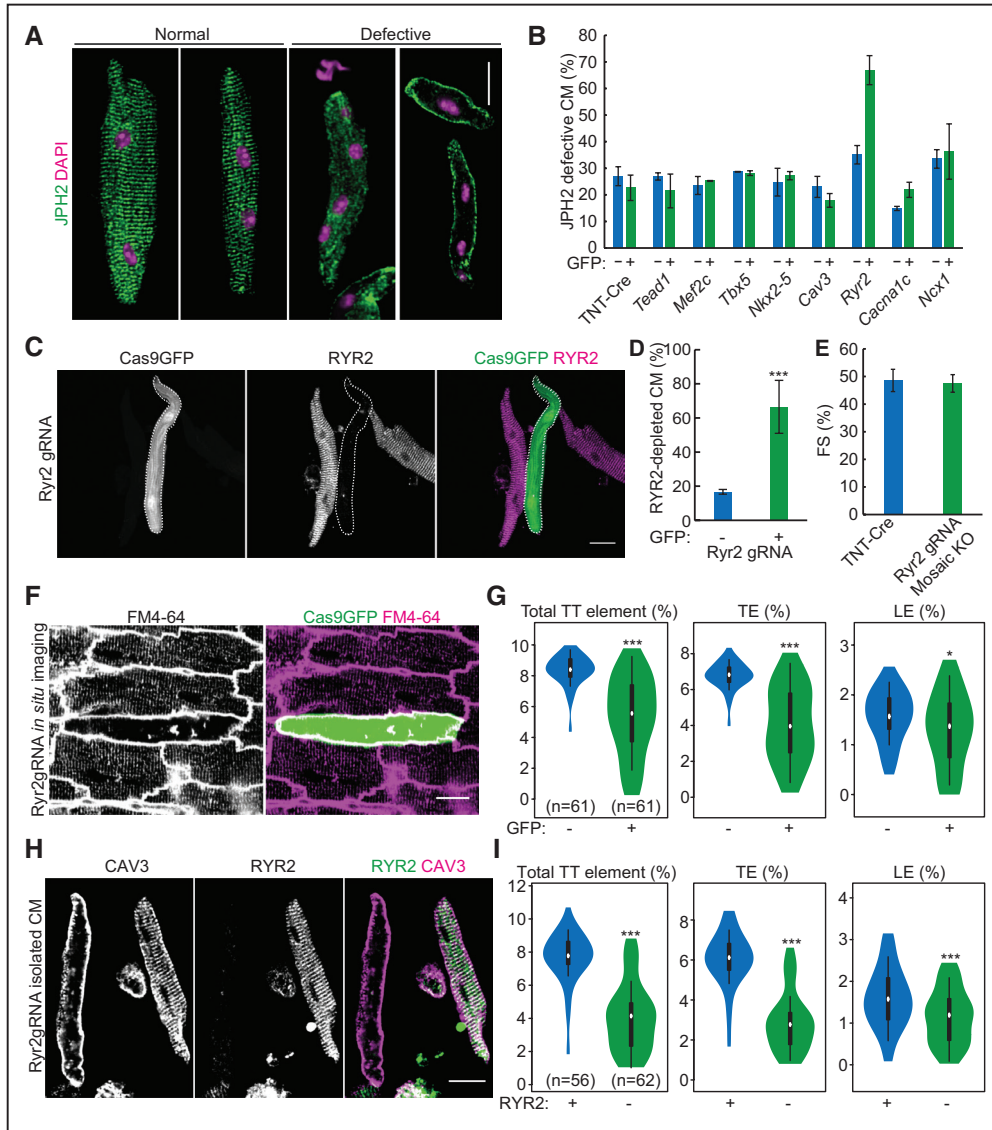


**Figure 8. CRISPR/Cas9/AAV9-based somatic mutagenesis (CASA)–based genetic screen identifies RYR2 (Ryanodine Receptor-2) as a novel transverse tubule (T-tubule) regulator.** **A**, Representative images of junctophilin-2 (JPH2) immunostaining patterns in isolated cardiac myocytes (CMs) that demonstrate normal and defective T-tubule organization. **B**, Quantification of JPH2 patterns in isolated postnatal day 21 (P21) CMs in which 8 candidate genes were individually and mosaically targeted. More than 50 CMs were counted per heart. n=3 hearts. **C**, Immunostaining of RYR2 demonstrates successful depletion of RYR2 in GFP+ CMs (delineated by dashed lines) that are infected by AAV-Ryr2gRNA. **D**, Quantification of RYR2 knockout efficiency. More than 50 CMs were counted per group. n=3 hearts. **E**, Fractional shortening (FS) of control and RYR2 mosaic knockout hearts. n=3. **F**, In situ T-tubule image of hearts under mosaic RYR2 knockout. **G**, AutoTT quantification of RYR2 mosaic knockout CMs. **H**, CAV3 and RYR2 immunostaining patterns in CMs isolated from hearts under RYR2 mosaic knockout. **I**, AutoTT quantification of CAV3 pattern in RYR2+ and RYR2- isolated CMs. In all images, scale bar=20 μm. Violin plots in **G** and **I** are as in Figure 2D. CMs were from 3 hearts. Student *t* test: \**P*<0.05; \*\**P*<0.01; \*\*\**P*<0.001. Column charts show mean±SD. LE indicates longitudinal element; TE, transverse element; Total TT element=TE+LE; and TNT, troponin-T.

controls. Efficient depletion of NKX2-5, TEAD1, RYR2, and CAV3 was validated by immunostaining (Online Figure VI; Figure 8C and 8D).

Through this screen, we found that RYR2 depletion caused dramatic disruption of the JPH2 staining pattern (Figure 8A and 8B). By contrast, the AAVs targeting the other 7 genes did not show this effect. Efficient depletion of RYR2 was observed in ≈65% of the AAV-infected GFP+ CMs (Figure 8C and 8D). Mice with mosaic RYR2 depletion in a minority of CMs (only ≈10% of total CMs were depleted of RYR2) maintained normal heart function (Figure 8E). Dramatic T-tubule disruption was

observed in GFP+ CMs under in situ T-tubule imaging, but GFP-neighboring cells retained normal T-tubule patterns (Figure 8F and 8G; see additional representative confocal z stacks in Online Movie IV). This phenotype was also confirmed in isolated CMs, as RYR2- CMs exhibited disrupted CAV3 staining pattern, whereas normal CAV3 pattern was observed in RYR2+ CMs (Figure 8H and 8I). The effect of RYR2 depletion on T-tubule structure staining pattern was reproduced with 2 additional independent pairs of gRNAs (Online Figure VII), which ruled out off-target effects. Together, these data show a novel cell-autonomous function of RYR2 in T-tubule maturation.

## Discussion

In this study, we combined AAV-mediated mosaic transduction and CRISPR/Cas9-based somatic mutagenesis to establish a powerful technical platform, named CASA AAV, which permits facile interrogation of cell-autonomous gene function in the postnatal heart. We also demonstrate the value of a genetic mosaic strategy to disentangle direct, cell-autonomous roles of a gene from changes that arise from effects on overall organ function. We anticipate that this strategy will allow the rapid and precise interrogation of gene function in the postnatal heart in diverse processes such as CM maturation, regeneration, and hypertrophy.

Somatic cardiac mutagenesis using a Cre-activated *Myh6-Cas9* allele was described previously.<sup>24</sup> Our study used the more widely available *Rosa26<sup>Cas9-GFP</sup>* mouse line,<sup>14</sup> which retains CM-selective gene inactivation in the heart because of the cardiotropic properties of AAV9 and cTNT-Cre-driven Cas9 activation. More importantly, our study focused on mosaic analysis of cell-autonomous phenotypes as a strength of the Cas9 somatic mutagenesis strategy. We performed foundational experiments that are required to fully exploit this strategy, including the demonstration that the dose of AAV mainly affects the frequency of transduced CMs but has only a small effect on the efficiency of gene inactivation among those CMs that are transduced. Furthermore, we provide data on the overall knockout efficiency of the system, demonstrate that tandem gRNAs targeting the same gene enhances knockout efficiency, and reveal the combination of mechanisms that collectively ensure a high knockout efficiency.

We combined CASA AAV with in situ T-tubule imaging to study the genetic regulation of CM maturation in vivo. At a full virus dose to maximize the transduction of CMs, CASA AAV fully recapitulated observations made using more traditional genetic models. For example, when JPH2 was depleted in a large fraction of CMs (*Jph2\_High* and *Jph2\_Full*), the heart exhibited ventricular dilatation, CM hypertrophy, and heart failure, which were all consistent with previous studies of *Mhy6-Cre; Jph2-shRNA* mice.<sup>2,8</sup> Dramatic T-tubule defects and Ca<sup>2+</sup> transient abnormalities in *Jph2\_High* mice also agreed with previous reports showing that organ-wide JPH2 knockdown caused heart failure and disrupted T-tubule organization and Ca<sup>2+</sup> handling.<sup>2,8</sup> Thus, this technology can faithfully detect the function of a given gene at both organ and single-cell levels, which provides an alternative and more rapid means to study the function of a given gene in the heart, compared with generation of transgenic or knockout mice.

A particular strength of the CASA AAV system is the ability to rapidly generate genetic mosaics, which permits precise delineation of gene function that is difficult to achieve using constitutive or even inducible knockout models. For example, because JPH2 depletion caused early-onset heart failure, which itself is associated with T-tubule disruption, studies in traditional JPH2 knockout mice were unable to disentangle the direct role of JPH2 on T-tubule maturation from its role to stabilize T-tubules in the face of cardiac dysfunction. By using a low dose of AAV to direct JPH2 depletion, we were able to separate the function of JPH2 in T-tubule maturation from its requirement to stabilize T-tubules in heart failure. In CMs

from *Jph2\_Low* mice that lacked JPH2 but had overall preserved heart function, we observed very mild T-tubule defects. However, as we increased the fraction of CMs that lack JPH2, we observed worsening T-tubule defects in both transduced and nontransduced CMs that paralleled the extent of heart dysfunction. These observations are consistent with previous studies<sup>2,31</sup> and suggest that widespread JPH2 depletion primarily affects T-tubule organization by impairing heart function. In failing hearts, we did observe that JPH2-depleted CMs had more severe T-tubule disruption than JPH2-replete CMs, supporting a role for JPH2 to stabilize T-tubules in the face of CM stress caused by heart dysfunction, as previously reported.<sup>31</sup> However, contrary to previous studies of JPH2 depletion done in the context of heart dysfunction,<sup>2,8</sup> our genetic mosaic approach shows that JPH2 has a minor cell-autonomous role in T-tubule maturation. This role of JPH2 was mirrored in its modest but measurable effects on Ca<sup>2+</sup> transient amplitude, which suggests that JPH2 may regulate RYR2 activation within Ca<sup>2+</sup> release units. A broader implication of these results is that studies of CM maturation or function need to use strategies such as genetic mosaicism to distinguish direct cell-autonomous gene function from effects of gene inactivation that occur secondary to organ function impairment.

Another advantage of performing mosaic mutagenesis is that it permits study of genes that are essential for animal survival. For example, because RYR2 is the core Ca<sup>2+</sup> channel that directly drives heart contraction, RYR2 knockout rapidly causes embryonic death,<sup>32</sup> precluding its detailed functional analysis in vivo in the postnatal heart. By contrast, through AAV-based mosaic knockout, we were able to study the in vivo function of RYR2 in adult CMs while maintaining normal heart function. This provided us with the unprecedented opportunity to identify a novel role of RYR2 in T-tubule organization. Thus, the CASA AAV platform opens the door to precisely investigate the cellular functions of essential genes in vivo, which otherwise would be technically inaccessible.

Our in vivo screen identified RYR2 as a previously undescribed regulator of T-tubule maturation. Further experiments will be required to define how RYR2 regulates T-tubule maturation. One possibility is that RYR2, located on junctional SR, serves a structural role by providing a scaffold that interacts with proteins on T-tubules. Another possibility is that normal Ca<sup>2+</sup> oscillations conducted through RYR2 are required to promote formation and maturation of T-tubules.

Because CRISPR/Cas9 provides the versatility to target most genes in the genome and CASA AAV avoids the time and resources required to generate genetically modified mice, this technology greatly expedites the use of genetic loss-of-function strategies to study gene function in the postnatal heart. In our hands, the whole procedure from gene selection to phenotypic characterization of T-tubules in knockout CM can be done within 6 weeks. As a result, we were able to perform the in vivo screen that led to identification of RYR2 as a novel T-tubule regulator. Thus, this technology is well suited for in vivo genetic screening for regulators of CM phenotypes, such as maturation and hypertrophy.

Adenoviral and AAV-mediated delivery of short hairpin RNAs (shRNAs) have been previously used to knockdown genes in postnatal CMs. Compared with short hairpin RNAs,

CASAAV has clear advantages. ShRNAs are unable to achieve complete protein depletion, and >70% depletion is often considered successful knockdown. ShRNAs must actively bind to target transcripts, so that knockdown depends on continued shRNA expression at sufficient levels compared with the endogenous transcript. With CASAAV, a subset of cells with homozygous truncating mutations will have complete protein depletion. Furthermore, CASAAV irreversibly modifies the genome, which makes gene knockdown irreversible, more potent than shRNAs, and likely accounts for the relative insensitivity of gene depletion efficiency among transduced cells to overall viral dose, a critical feature for the mosaic strategy.

The CASAAV system has some limitations. First, we are unaware of efficient homology-directed repair in terminally differentiated cells, making targeted knockin mutations infeasible. Second, as with RNA interference-based knockdown strategies, one should be cognizant of potential off-target activity and control for this possibility by careful gRNA design and, optimally, use of  $\geq 2$  independent gRNA pairs to target the same gene. Third, the possibility of gain-of-function mutations should be considered, for example, if the gRNA leads to C-terminal truncation and a dominant negative N-terminal protein fragment. We used gRNAs targeting near the N terminus of genes to minimize this possibility. Fourth, for the mosaic strategy to be successful, one needs means to identify individual cells that have undergone gene inactivation. Immunostaining with a high-quality antibody is one such assay. Alternatively, if the fraction of cells that have undergone gene depletion is sufficiently high, one can use GFP from *Rosa26<sup>Cas9-GFP</sup>* as a surrogate marker. When doing so, one should also be aware that a low fraction of GFP-negative cells also could have undergone Cas9 mutagenesis but have lost GFP expression. Typically, this can be overcome by studying a large number of single cells.

In summary, we have developed a rapid and powerful technical platform for gene inactivation in postnatal CMs. This platform is particularly well suited for genetic mosaic analysis of genes to define the cell-autonomous functions. In the future, we anticipate that the capabilities of this system will be further extended by pairing it with single-cell functional phenotyping and single-cell RNA-seq.

### Acknowledgments

Y. Guo and N.J. VanDusen contributed equally to this article. Y. Guo designed and performed experiments and collected and analyzed data. N.J. VanDusen developed the somatic mutagenesis adeno-associated virus vector and contributed to data collection and analysis. L. Zhang, W. Gu, Q. Ma, B.D. Jardin, and D. Zhang contributed to the creation of reagents and collection of data. N.J. VanDusen and S. Guatimosim performed  $\text{Ca}^{2+}$  imaging. I. Sethi and G.-C. Yuan analyzed Amplicon-Seq data. A. Guo and L.-S. Song contributed to analysis of T-tubule morphology with AutoTT software. Y. Guo and N.J. VanDusen wrote the article. W.T. Pu directed the overall project, analyzed data, and edited the article.

### Sources of Funding

The project was supported by UM1 HL098166, R01 HL116461, and U01HL131003 from the National Heart, Lung, and Blood Institute. L.-S. Song was supported by R01HL090905 and R01HL130464. N.J. VanDusen was supported by T32HL007572 and F32HL13423501. S. Guatimosim was a recipient of a

Coordenação de Aperfeiçoamento de Pessoal de Nível Superior fellowship and funded by Conselho Nacional de Desenvolvimento Científico e Tecnológico and Fundação de Amparo à Pesquisa do Estado de Minas Gerais. The content is solely the responsibility of the authors and does not necessarily represent the official views of the National Heart, Lung, and Blood Institute or the National Institutes of Health.

### Disclosures

None.

### References

1. Yang X, Pabon L, Murry CE. Engineering adolescence: maturation of human pluripotent stem cell-derived cardiomyocytes. *Circ Res*. 2014;114:511–523. doi: 10.1161/CIRCRESAHA.114.300558.
2. Chen B, Guo A, Zhang C, Chen R, Zhu Y, Hong J, Kutschke W, Zimmerman K, Weiss RM, Zingman L, Anderson ME, Wehrens XH, Song LS. Critical roles of junctophilin-2 in T-tubule and excitation-contraction coupling maturation during postnatal development. *Cardiovasc Res*. 2013;100:54–62. doi: 10.1093/cvr/cvt180.
3. Sallé L, Brette F. T-tubules: a key structure of cardiac function and dysfunction. *Arch Mal Coeur Vaiss*. 2007;100:225–230.
4. Orchard C, Brette F. T-Tubules and sarcoplasmic reticulum function in cardiac ventricular myocytes. *Cardiovasc Res*. 2008;77:237–244. doi: 10.1093/cvr/cvm002.
5. Beavers DL, Landstrom AP, Chiang DY, Wehrens XH. Emerging roles of junctophilin-2 in the heart and implications for cardiac diseases. *Cardiovasc Res*. 2014;103:198–205. doi: 10.1093/cvr/cvu151.
6. Landstrom AP, Beavers DL, Wehrens XH. The junctophilin family of proteins: from bench to bedside. *Trends Mol Med*. 2014;20:353–362. doi: 10.1016/j.molmed.2014.02.004.
7. Takeshima H, Komazaki S, Nishi M, Iino M, Kangawa K. Junctophilins: a novel family of junctional membrane complex proteins. *Mol Cell*. 2000;6:11–22.
8. Reynolds JO, Chiang DY, Wang W, Beavers DL, Dixit SS, Skapura DG, Landstrom AP, Song LS, Ackerman MJ, Wehrens XH. Junctophilin-2 is necessary for T-tubule maturation during mouse heart development. *Cardiovasc Res*. 2013;100:44–53. doi: 10.1093/cvr/cvt133.
9. Wei S, Guo A, Chen B, Kutschke W, Xie YP, Zimmerman K, Weiss RM, Anderson ME, Cheng H, Song LS. T-tubule remodeling during transition from hypertrophy to heart failure. *Circ Res*. 2010;107:520–531. doi: 10.1161/CIRCRESAHA.109.212324.
10. Poláková E, Sobie EA. Alterations in T-tubule and dyad structure in heart disease: challenges and opportunities for computational analyses. *Cardiovasc Res*. 2013;98:233–239. doi: 10.1093/cvr/cvt026.
11. Prendiville TW, Guo H, Lin Z, Zhou P, Stevens SM, He A, VanDusen N, Chen J, Zhong L, Wang DZ, Gao G, Pu WT. Novel roles of GATA4/6 in the postnatal heart identified through temporally controlled, cardiomyocyte-specific gene inactivation by adeno-associated virus delivery of cre recombinase. *PLoS One*. 2015;10:e0128105. doi: 10.1371/journal.pone.0128105.
12. Swiech L, Heidenreich M, Banerjee A, Habib N, Li Y, Trombetta J, Sur M, Zhang F. In vivo interrogation of gene function in the mammalian brain using CRISPR-Cas9. *Nat Biotechnol*. 2015;33:102–106. doi: 10.1038/nbt.3055.
13. Lin Z, von Gise A, Zhou P, Gu F, Ma Q, Jiang J, Yau AL, Buck JN, Gouin KA, van Gorp PR, Zhou B, Chen J, Seidman JG, Wang DZ, Pu WT. Cardiac-specific YAP activation improves cardiac function and survival in an experimental murine MI model. *Circ Res*. 2014;115:354–363. doi: 10.1161/CIRCRESAHA.115.303632.
14. Platt RJ, Chen S, Zhou Y, et al. CRISPR-Cas9 knockin mice for genome editing and cancer modeling. *Cell*. 2014;159:440–455. doi: 10.1016/j.cell.2014.09.014.
15. O'Connell TD, Rodrigo MC, Simpson PC. Isolation and culture of adult mouse cardiac myocytes. *Methods Mol Biol*. 2007;357:271–296.
16. He A, Pu WT. Genome-wide location analysis by pull down of in vivo biotinylated transcription factors. *Curr Protoc Mol Biol*. 2010;92:21.20.21.20.1–21.20.15. doi: 10.1002/0471142727.mb2120s92.
17. Pinello L, Canver MC, Hoban MD, Orkin SH, Kohn DB, Bauer DE, Yuan GC. Analyzing CRISPR genome-editing experiments with CRISPResso. *Nat Biotechnol*. 2016;34:695–697. doi: 10.1038/nbt.3583.
18. Guo Y, Zheng Y. Lamins position the nuclear pores and centrosomes by modulating dynein. *Mol Biol Cell*. 2015;26:3379–3389. doi: 10.1091/mbc.E15-07-0482.

19. Guo Y, Kim Y, Shimi T, Goldman RD, Zheng Y. Concentration-dependent lamin assembly and its roles in the localization of other nuclear proteins. *Mol Biol Cell*. 2014;25:1287–1297. doi: 10.1091/mbc.E13-11-0644.
20. Guo A, Song LS. AutoTT: automated detection and analysis of T-tubule architecture in cardiomyocytes. *Biophys J*. 2014;106:2729–2736. doi: 10.1016/j.bpj.2014.05.013.
21. Jinek M, Chylinski K, Fonfara I, Hauer M, Doudna JA, Charpentier E. A programmable dual-RNA-guided DNA endonuclease in adaptive bacterial immunity. *Science*. 2012;337:816–821. doi: 10.1126/science.1225829.
22. Cong L, Ran FA, Cox D, Lin S, Barretto R, Habib N, Hsu PD, Wu X, Jiang W, Marraffini LA, Zhang F. Multiplex genome engineering using CRISPR/Cas systems. *Science*. 2013;339:819–823. doi: 10.1126/science.1231143.
23. Mali P, Yang L, Esvelt KM, Aach J, Guell M, DiCarlo JE, Norville JE, Church GM. RNA-guided human genome engineering via Cas9. *Science*. 2013;339:823–826. doi: 10.1126/science.1232033.
24. Carroll KJ, Makarewich CA, McAnally J, Anderson DM, Zentilin L, Liu N, Giacca M, Bassel-Duby R, Olson EN. A mouse model for adult cardiac-specific gene deletion with CRISPR/Cas9. *Proc Natl Acad Sci USA*. 2016;113:338–343. doi: 10.1073/pnas.1523918113.
25. Pacak CA, Mah CS, Thattaliyath BD, Conlon TJ, Lewis MA, Cloutier DE, Zolotukhin I, Tarantal AF, Byrne BJ. Recombinant adeno-associated virus serotype 9 leads to preferential cardiac transduction in vivo. *Circ Res*. 2006;99:e3–e9. doi: 10.1161/01.RES.0000237661.18885.f6.
26. Sander JD, Joung JK. CRISPR-Cas systems for editing, regulating and targeting genomes. *Nat Biotechnol*. 2014;32:347–355. doi: 10.1038/nbt.2842.
27. Hong T, Yang H, Zhang SS, Cho HC, Kalashnikova M, Sun B, Zhang H, Bhargava A, Grabe M, Olgin J, Gorelik J, Marbán E, Jan LY, Shaw RM. Cardiac BIN1 folds T-tubule membrane, controlling ion flux and limiting arrhythmia. *Nat Med*. 2014;20:624–632. doi: 10.1038/nm.3543.
28. Mamanova L, Coffey AJ, Scott CE, Kozarewa I, Turner EH, Kumar A, Howard E, Shendure J, Turner DJ. Target-enrichment strategies for next-generation sequencing. *Nat Methods*. 2010;7:111–118. doi: 10.1038/nmeth.1419.
29. Chang YF, Imam JS, Wilkinson MF. The nonsense-mediated decay RNA surveillance pathway. *Annu Rev Biochem*. 2007;76:51–74. doi: 10.1146/annurev.biochem.76.050106.093909.
30. Chen B, Zhang C, Guo A, Song LS. In situ single photon confocal imaging of cardiomyocyte T-tubule system from Langendorff-perfused hearts. *Front Physiol*. 2015;6:134. doi: 10.3389/fphys.2015.00134.
31. Guo A, Zhang X, Iyer VR, Chen B, Zhang C, Kutschke WJ, Weiss RM, Franzini-Armstrong C, Song LS. Overexpression of junctophilin-2 does not enhance baseline function but attenuates heart failure development after cardiac stress. *Proc Natl Acad Sci USA*. 2014;111:12240–12245. doi: 10.1073/pnas.1412729111.
32. Takeshima H, Komazaki S, Hirose K, Nishi M, Noda T, Iino M. Embryonic lethality and abnormal cardiac myocytes in mice lacking ryanodine receptor type 2. *EMBO J*. 1998;17:3309–3316. doi: 10.1093/emboj/17.12.3309.

# Circulation Research

JOURNAL OF THE AMERICAN HEART ASSOCIATION



## Analysis of Cardiac Myocyte Maturation Using CASA AV, a Platform for Rapid Dissection of Cardiac Myocyte Gene Function In Vivo

Yuxuan Guo, Nathan J. VanDusen, Lina Zhang, Weiliang Gu, Isha Sethi, Silvia Guatimosim, Qing Ma, Blake D. Jardin, Yulan Ai, Donghui Zhang, Biyi Chen, Ang Guo, Guo-Cheng Yuan, Long-Sheng Song and William T. Pu

*Circ Res.* 2017;120:1874-1888; originally published online March 29, 2017;  
doi: 10.1161/CIRCRESAHA.116.310283

*Circulation Research* is published by the American Heart Association, 7272 Greenville Avenue, Dallas, TX 75231  
Copyright © 2017 American Heart Association, Inc. All rights reserved.  
Print ISSN: 0009-7330. Online ISSN: 1524-4571

The online version of this article, along with updated information and services, is located on the World Wide Web at:

<http://circres.ahajournals.org/content/120/12/1874>

Data Supplement (unedited) at:

<http://circres.ahajournals.org/content/suppl/2017/03/29/CIRCRESAHA.116.310283.DC1>

**Permissions:** Requests for permissions to reproduce figures, tables, or portions of articles originally published in *Circulation Research* can be obtained via RightsLink, a service of the Copyright Clearance Center, not the Editorial Office. Once the online version of the published article for which permission is being requested is located, click Request Permissions in the middle column of the Web page under Services. Further information about this process is available in the [Permissions and Rights Question and Answer](#) document.

**Reprints:** Information about reprints can be found online at:  
<http://www.lww.com/reprints>

**Subscriptions:** Information about subscribing to *Circulation Research* is online at:  
<http://circres.ahajournals.org/subscriptions/>

## SUPPLEMENTAL MATERIAL

- A. Detailed Materials and Methods
- B. Supplemental References
- C. Online Tables
  - Online Table I. gRNA sequences for CRISPR/Cas9
  - Online Table II. Primers
  - Online Table III. Antibody and Dye List
- D. Online Figures
  - Online Figure I. AAV ITR vector for delivery of tandem guide RNAs and cTNT-Cre
  - Online Figure II. Distribution of GFP and tdTomato reporters in Rosa26<sup>Cas9GFP/tdTomato</sup> mice after treatment with AAV9:TNT-Cre
  - Online Figure III. Frame-shift mutations induced by Jph2gRNA-directed Cas9 cleavage followed by NHEJ
  - Online Figure IV. JPH2 immunoblot of FACS-sorted GFP+ CMs treated with TNT-Cre or Jph2(gRNA1+2) AAV.
  - Online Figure V. JPH2 depletion did not cell-autonomously disrupt sarcomere organization
  - Online Figure VI. Depletion of NKX2-5, TEAD1 and CAV3 by CASA AV
  - Online Figure VII. Mosaic RYR2 depletion using multiple gRNA pairs disrupts T-tubule structure.
- E. Online Movies
  - Online Movie I. *In situ* T-tubule imaging in a Jph2\_Low heart
  - Online Movie II. *In situ* T-tubule imaging in a Jph2\_Mid heart
  - Online Movie III. *In situ* T-tubule imaging in a Jph2\_High heart
  - Online Movie IV. *In situ* T-tubule imaging in a RYR2 mosaic mutagenesis heart

## A. Detailed Materials and Methods

### Plasmid construction

AAV-U6-TnT-Cre ITR plasmid was developed by modification of PX552 (Addgene #60958). PX552 was digested with XbaI and HindIII to remove the hSyn promoter and eGFP cDNA. A 414 bp chicken cardiac Troponin T promoter +  $\beta$  Globin intron and Cre cDNA was PCR amplified with primers tagged with SpeI 5' and HindIII 3' from an AAV-TnT-Cre plasmid reported previously<sup>1</sup>. The TnT-Cre amplicon was then cloned into the digested PX552 vector. Addition of a second U6 promoter and gRNA scaffold was achieved by cloning the second U6 promoter and a 5' AarI site into the MluI site upstream of the first U6 promoter. An additional AarI site and the second gRNA scaffold was then cloned into the same MluI site. See Online Fig. 1 for the map of gRNA cloning strategy this plasmid. gRNAs (Online Table I) were designed using an online tool (<http://crispr.mit.edu/>) and cloned into the first or second U6 promoter cloning sites.

### AAV9 production

AAV9 was prepared using standard protocols<sup>2</sup> with modifications. In brief, AAV-ITR plasmids, AAV9-Rep-Cap, and pHelper (pAd-deltaF6, Penn Vector Core) plasmids were produced by maxiprep (Invitrogen, K210017). Triple transfection into AAV293 cells (Agilent, 240073) was performed using PEI transfection reagent (Polysciences, 23966-2). 60h after transfection, cells were scraped off of plates, resuspended in lysis buffer (20 mM Tris pH 8, 150 mM NaCl, 1 mM MgCl<sub>2</sub>, 50  $\mu$ g/ml Benzonase) and lysed by three freeze-thaw cycles. AAV9 was precipitated by PEG8000 (VWR, 97061-100) and re-suspended in lysis buffer. AAV was purified in a density gradient (Cosmo Bio USA, AXS-1114542) by ultracentrifugation (Beckman, XL-90) with a VTi-50 rotor and concentrated in PBS using a 100 kD filter tube (Fisher Scientific, UFC910024). AAV titer was quantified by Q-PCR (primer sequences in Online Table II) using a fragment of the TNT promoter DNA to make a standard curve.

### Animal experiments

All animal procedures were approved by the Institutional Animal Care and Use Committee of Boston Children's Hospital. Rosa<sup>Cas9GFP/Cas9GFP</sup> and Rosa<sup>tdTomato/tdTomato</sup> mice were acquired from the Jackson Laboratory.

To inject AAV into P1 pups, the body weight of the animals was measured and the pups were anesthetized in an isoflurane chamber. The amount of AAV was calculated according to body weight and injected subcutaneously.

Echocardiography was performed on a VisualSonics Vevo 2100 with Vevostrain software. Animals were awake during this procedure and held in a standard handgrip. Echocardiography was performed blinded to treatment group.

### Gene expression analysis

Total RNA was purified from the heart apex using PureLink RNA Mini kit (Ambion, 12183025). Genomic DNA removal from RNA and reverse transcription was performed using QuantiTech reverse transcription kit (Qiagen, 205311). Real-time PCR was performed using an ABI 7500 thermocycler with Power SYBR Green PCR kit (ThermoFisher, 4368702). Primers are listed in Online Table II.

### Amplicon Sequencing

Primers that were used to generate DNA libraries are listed in Online Table II. DNA library construction protocol was modified from our previous protocol<sup>3</sup>. In brief, targeted cDNA sequences were amplified by PCR using Phusion High-Fidelity DNA polymerase (NEB, M0530S). The amplicons were next phosphorylated by T4 polynucleotide kinase (NEB, M0201S) and adenylated by Klenow fragment (3'-5' exo-) (NEB, M0212S). Adaptor primers were phosphorylated, annealed and ligated to both ends of the amplicons through T-A ligation using Quick Ligation kit (NEB, M2200S). Multiplexing primers were next used to barcode and PCR amplify the DNA libraries. After each step above, DNA was purified by AMPure XP beads (Beckman, A63881) under 1.6X conditions. Then an equal amount of each library was pooled together and gel purified to remove free primers and primer dimers. 250 bp paired end sequencing was performed on a MiSeq Sequencer (Illumina).

Amplicon-Seq reads were first quality controlled and trimmed to remove adapter sequences (Multiplexing adapter 1: p-GATCGGAAGAGCACACGTCT, Multiplexing adapter 2: ACACTCTTTCCTACACGACGCTCTCCGATCT) using Trim Galore (a wrapper tool around Cutadapt<sup>4</sup> and FastQC) ([http://www.bioinformatics.babraham.ac.uk/projects/trim\\_galore/](http://www.bioinformatics.babraham.ac.uk/projects/trim_galore/)). Insertions/deletions in the trimmed sequencing libraries were then quantified using CRISPResso software<sup>5</sup> run with the optional parameters -g, -c and --hide\_mutations\_outside\_window\_NHEJ. For analyzing amplicon 1&2, we ran CRISPResso in single-end mode ( using read1 files) as the read length was longer than the amplicon size. However amplicon 3 is 512 bp in size and therefore we analyzed it by utilizing the paired end option (using parameter -r2 to specify read2 files).

### Cardiomyocyte isolation and culture

Cardiomyocytes were isolated by Langendorff perfusion using an established protocol<sup>6</sup> with modifications. In brief, heparin-injected mice were anesthetized in an isoflurane chamber. Hearts were isolated and cannulated onto the perfusion apparatus. Perfusion buffer [10 mM Hepes (pH 7.4), 120.4 mM NaCl, 14.7 mM KCl, 0.6 mM KH<sub>2</sub>PO<sub>4</sub>, 0.6 mM Na<sub>2</sub>HPO<sub>4</sub>, 1.2 mM MgSO<sub>4</sub>, 4.6 mM NaHCO<sub>3</sub>, 30 mM Taurine, 10 mM 2,3-butanedione monoxime, 5.5 mM glucose] was pumped into the heart to clear blood and equilibrate the organ. Retrograde perfusion of collagenase II (Worthington, LS004177) was performed in the heart for 10 min at 37 °C to dissociate

cardiomyocytes. Heart apex was cut from the digested heart, manually dissociated into single cardiomyocytes in 10% FBS/perfusion buffer, and filtered through a 100 µm cell strainer to remove undigested tissues. The isolated cardiomyocytes were concentrated by 20 x g low-speed centrifugation for 4 min and re-suspended in short-term culture medium (DMEM (Gibco), 10% FBS, pen/strep (Gibco), 10 µM Blebbistatin). Cardiomyocytes were cultured on laminin-coated coverslips in culture medium for <1 h at 37 °C with 5% CO<sub>2</sub> before fixation.

### Flow Cytometry

For flow cytometry analysis, freshly isolated CMs were passed through a 100 µm cell strainer and centrifuged at 20 x g for 5 minutes at room temperature. Non-myocytes in the supernatant were discarded and the pelleted CMs were resuspended in 2.5 ml of PBS. Fluorescence data were collected on a Propel Laboratories Avalon cytometer with a 100 µm nozzle and standard GFP/RFP filter sets. Data were further analyzed using BioRad ProSort software.

For FACS, CMs from each heart were passed through a 100 µm cell strainer, centrifuge at 20 x g for 5min at RT, resuspended in ~1ml perfusion buffer. FACS were performed using a BD Ariall SORP cell sorter with a 100 µm nozzle. GFP+ CMs were collected in 1.5 ml Eppendorff tubes with cold perfusion buffer.

### Histology analysis

After mice were euthanized by CO<sub>2</sub>, body weight was measured using a digital benchtop scale (Sartorius, AY123). Hearts were removed, gently blotted to remove liquid, and weighed using an analytical balance (Fisher Science Education). Bright-field images of whole hearts were taken under a dissection microscope (Zeiss, SteREO Discovery V8). Images of hearts that were isolated from mice with similar body weights (<10% difference) were put together for comparison.

Hearts were fixed by 4% paraformaldehyde overnight at 4 °C and cryoprotected by washing in 15% followed by 30% sucrose. Hearts were embedded in tissue freezing medium (General Data, TFM-5). 10 µm cryo-sections were cut using a cryostat (Thermo Scientific, Microm HM 550).

Hematoxylin & eosin staining was performed on cryo-sections. Sections were first air dried at room temperature, stained with 0.1% Mayers Hematoxylin for 10 min and rinsed in water for 5 min. Next the sections were dipped in 0.5% Eosin for 2 min and rinsed in water for 2 min. Then the sections were dipped in 50%, 70%, 95%, 100% ethanol and Xylene. After air drying, the sections were mounted using VectaMount permanent mounting medium (Vector Laboratories, H5000).

### Immunofluorescence

Isolated cardiomyocytes were immunostained as described previously<sup>7,8</sup>. In brief, cardiomyocytes in culture were fixed on coverslips by 4% paraformaldehyde/PBS for 10

min, permeabilized by 0.1% Triton-100/PBS for 10 min, and blocked in 4% BSA/PBS at room temperature for 1 h. Then the cells were incubated with primary antibodies diluted in blocking buffer overnight at 4 °C. After three 5 min washes with blocking buffer, the cells were incubated with secondary antibodies and dyes at room temperature for 2 h. Then the cells were washed with PBS three times and mounted with ProLong Diamond antifade mountant (Invitrogen, 36961)

To immunostain tissue sections, frozen sections were first warmed to room temperature, incubated with 0.1% Triton-100/PBS for 10 min, and blocked with 4% normal donkey serum/PBS at room temperature for 2 h. Then the cells were incubated with primary antibodies diluted in blocking buffer overnight at 4 degree. After three 15 min washes with blocking buffer, the cells were incubated with secondary antibodies with/without WGA and/or DAPI at room temperature for 2 h. Then the sections were washed with PBS for 15 min/each for three times and mounted with ProLong Diamond antifade mountant (Invitrogen, 36961)

All antibodies and dyes used in this study are listed in Online Table III.

#### Western blot

FACS sorted CMs were lysed in 2X SDS sample buffer at 2000 cell/ul concentration to normalize protein contents. After boiled for 5 min, 5 µl cell lysate of each sample was separated on a 4%-12% gradient gel (Invitrogen, Bolt gels, NW04122BOX), transferred to a PDVF membrane, and blocked by 4% milk/TBST. Primary antibodies were incubated with the membrane overnight at 4°C, followed by four 15min TBST washes. HRP-conjugated secondary antibodies were probed for 1~2h at RT, followed by four 15 min TBST washes. After adding Immobilon Western chemiluminescent HRP substrate (Millipore, WBKLS0500), chemiluminescence were detected by a Li-Cor C-DiGit blot scanner.

All antibodies used in this study are listed in Online Table III.

#### In situ confocal T-tubule imaging

*In situ* T-tubule imaging was performed following a published protocol<sup>9</sup> with modifications. In brief, hearts were dissected from euthanized animals and cannulated on a Langendorff apparatus. 100 µg/ml FM 4-64 (Invitrogen, 13320) was loaded into the heart by retrograde perfusion at room temperature for 10 min. The heart was next removed from the perfusion system, positioned on a glass-bottom dish, and immediately imaged by confocal microscopy.

#### Microscopy and image analysis

All bright-field images was taken under a stereomicroscope (Zeiss SteREO Discovery V8) with an AxioCam MRc camera. All confocal fluorescence images were taken using Olympus FV1000 inverted laser scanning confocal microscope equipped with an EM-CCD camera. A 60X/1.3 silicone-oil objective was used to image all

intracellular structures including t-tubule, sarcomere and nuclei. A 10X air objective was used to image whole tissue sections. Brightness and contrast were adjusted using ImageJ. All cell-counting-based quantification was performed manually under Nikon Eclipse 90i microscope with a Plan Fluor 40x/0.75 objective.

For JPH2 immunofluorescence intensity measurement on single cells, all cells were cultured, stained and imaged side-by-side under the same conditions on the same day. Cell boundary was manually drawn on maximally projected images and the average pixel intensity within the outlined images was measured using ImageJ. Background intensity was determined by measuring cell-free areas and was subtracted from the JPH2 average intensity.

Quantification of T-tubule and sarcomere were performed using AutoTT v1.0 software<sup>10</sup>.

### Intracellular Ca<sup>2+</sup> imaging

Intracellular Ca<sup>2+</sup> recordings were performed after loading CMs with Rhod-2 AM (8 µmol/L, Molecular Probes) for 30 min. After loading, CMs were subsequently washed with normal Tyrode solution (NaCl, 140 mM; KCl, 4 mM; MgCl<sub>2</sub>, 1 mM; CaCl<sub>2</sub>, 1.8 mM; Glucose, 10 mM; and HEPES, 5 mM, pH = 7.4, adjusted with NaOH) to remove the excess dye for 20 min. Cells were electrically stimulated at 1 Hz to produce steady-state conditions. All image data were acquired in the line scanning mode along the long axis of the cell. Line scan was positioned in the cytosol, avoiding the nuclear area. Ca<sup>2+</sup> levels were reported as F/F<sub>0</sub>, where F<sub>0</sub> is the resting Ca<sup>2+</sup> fluorescence. A Olympus FV1000 inverted laser scanning confocal microscope with a 60X/1.3 silicone-oil objective was used for confocal fluorescence imaging by line scan.

## B. Supplemental References

1. Prendiville TW, Guo H, Lin Z, Zhou P, Stevens SM, He A, VanDusen N, et al. Novel Roles of GATA4/6 in the Postnatal Heart Identified through Temporally Controlled, Cardiomyocyte-Specific Gene Inactivation by Adeno-Associated Virus Delivery of Cre Recombinase. *PLoS One*. 2015;10:e0128105.
2. Grieger JC, Choi VW, Samulski RJ. Production and characterization of adeno-associated viral vectors. *Nat Protoc*. 2006;1:1412–1428.
3. He A, Pu WT. Genome-wide location analysis by pull down of in vivo biotinylated transcription factors. *Curr Protoc Mol Biol*. 2010;Chapter 21:Unit 21.20.
4. Martin M. Cutadapt removes adapter sequences from high-throughput sequencing reads. *EMBnet.journal*. 2011;17:10–12.
5. Pinello L, Canver MC, Hoban MD, Orkin SH, Kohn DB, Bauer DE, Yuan G-C. Analyzing CRISPR genome-editing experiments with CRISPResso. *Nat Biotechnol*. 2016;34:695–697.
6. O’Connell TD, Rodrigo MC, Simpson PC. Isolation and Culture of Adult Mouse Cardiac Myocytes. In: Vivanco F, editor. Cardiovascular Proteomics. Humana Press; p. 271–296.
7. Guo Y, Kim Y, Shimi T, Goldman RD, Zheng Y. Concentration-dependent lamin assembly and its roles in the localization of other nuclear proteins. *Mol Biol Cell*. 2014;25:1287–1297.
8. Guo Y, Zheng Y. Lamins position the nuclear pores and centrosomes by modulating dynein. *Mol Biol Cell*. 2015;26:3379–3389.
9. Chen B, Zhang C, Guo A, Song L-S. In situ single photon confocal imaging of cardiomyocyte T-tubule system from Langendorff-perfused hearts. *Front Physiol*. 2015;6:134.
10. Guo A, Song L-S. AutoTT: automated detection and analysis of T-tubule architecture in cardiomyocytes. *Biophys J*. 2014;106:2729–2736.

### C. Online Tables

Online Table I. gRNA design for CRISPR/Cas9 mutagenesis

Gene target	gRNA target 1	gRNA target 2
<i>tdTomato</i>	ggcgagggccgcccctacga	n/a
<i>Jph2</i>	gatgatggcggggcgtattg	attccaagtgcctcgtact
<i>Nkx2-5</i>	tggcctcgaggcgcgcagac	gaccctcgggcgataaaaa
<i>Tead1</i>	ccgattgacaacgacgcgga	tggctatctatccgccgtgt
<i>Mef2c</i>	acaacgagccgcacgagagc	ccatgtcagtgctggcgtag
<i>Tbx5</i>	tggcctggcgcgacgcctc	caagtctccatcatccccgc
<i>Ryr2</i>	cctgcagggcccgtactgac	gtgcagatagacagggtccgg
<i>Ryr2 Pair2</i>	cctgtcagtagcgggcccctgc	gcacaaagggtgcagatagac
<i>Ryr2 Pair3</i>	tgagggtggttctgcagtgca	tgcttggcagcagaaggatt
<i>Cav3</i>	gaccgaagagcacacggatc	cattgatggttcttggggtag
<i>Cacna1c</i>	agccatcgatgccgcccggc	ttatgcacgccctccggata
<i>Ncx1</i>	tgtttcaatgggatttcgac	ctctcgctcacgtgagtag

Online Table II. Primers

Primers for amplicon sequencing		
	primer 1	primer 2
Amplicon 1 PCR	ctagcccgggtggtgagtcta	gtattcacctggcccttgg
Amplicon 2 PCR	gacatgggcttggcatagag	gttggtgaattggccttgat
Amplicon 3 PCR	ctagcccgggtggtgagtcta	gttggtgaattggccttgat
Adaptor primers	gatcgggaagagcacacgtct	acactctttccctacacgacgctcttccgatct
universal barcoding primer	aatgatacggcgaccaccgagatctacactctttccctacacgacgctcttccgatct	
multiplexing barcoding primer (where bold indicates barcodes designed according to NEB 96-multiplexing kit, E6609)		
1	caagcagaagacggcatacagagat <b>gtcggtaa</b> gtgactggagttcagacgtgtgctcttccgatct	
2	caagcagaagacggcatacagagat <b>aggctact</b> gtgactggagttcagacgtgtgctcttccgatct	
3	caagcagaagacggcatacagagat <b>gaatccga</b> gtgactggagttcagacgtgtgctcttccgatct	
4	caagcagaagacggcatacagagat <b>gtaccttg</b> gtgactggagttcagacgtgtgctcttccgatct	
5	caagcagaagacggcatacagagat <b>catgaggag</b> gtgactggagttcagacgtgtgctcttccgatct	
6	caagcagaagacggcatacagagat <b>tgactgac</b> gtgactggagttcagacgtgtgctcttccgatct	
7	caagcagaagacggcatacagagat <b>cgatttcgg</b> gtgactggagttcagacgtgtgctcttccgatct	
8	caagcagaagacggcatacagagat <b>ctcctaga</b> gtgactggagttcagacgtgtgctcttccgatct	
9	caagcagaagacggcatacagagat <b>tagttgcg</b> gtgactggagttcagacgtgtgctcttccgatct	
10	caagcagaagacggcatacagagat <b>gagatacgg</b> gtgactggagttcagacgtgtgctcttccgatct	
11	caagcagaagacggcatacagagat <b>agggttac</b> gtgactggagttcagacgtgtgctcttccgatct	
12	caagcagaagacggcatacagagat <b>taatgccc</b> gtgactggagttcagacgtgtgctcttccgatct	
13	caagcagaagacggcatacagagat <b>tcagacga</b> gtgactggagttcagacgtgtgctcttccgatct	
14	caagcagaagacggcatacagagat <b>gataggct</b> gtgactggagttcagacgtgtgctcttccgatct	
15	caagcagaagacggcatacagagat <b>tggtacag</b> gtgactggagttcagacgtgtgctcttccgatct	
16	caagcagaagacggcatacagagat <b>caaggtct</b> gtgactggagttcagacgtgtgctcttccgatct	
17	caagcagaagacggcatacagagat <b>gctatcct</b> gtgactggagttcagacgtgtgctcttccgatct	
18	caagcagaagacggcatacagagat <b>atggaagg</b> gtgactggagttcagacgtgtgctcttccgatct	
19	caagcagaagacggcatacagagat <b>tcaaggac</b> gtgactggagttcagacgtgtgctcttccgatct	
20	caagcagaagacggcatacagagat <b>gttacgca</b> gtgactggagttcagacgtgtgctcttccgatct	
21	caagcagaagacggcatacagagat <b>agtctgtg</b> gtgactggagttcagacgtgtgctcttccgatct	
22	caagcagaagacggcatacagagat <b>gcacgtaa</b> gtgactggagttcagacgtgtgctcttccgatct	
23	caagcagaagacggcatacagagat <b>aaccttgg</b> gtgactggagttcagacgtgtgctcttccgatct	
24	caagcagaagacggcatacagagat <b>attgctgtg</b> gtgactggagttcagacgtgtgctcttccgatct	
25	caagcagaagacggcatacagagat <b>acctgga</b> gtgactggagttcagacgtgtgctcttccgatct	
26	caagcagaagacggcatacagagat <b>ggagatga</b> gtgactggagttcagacgtgtgctcttccgatct	
27	caagcagaagacggcatacagagat <b>gtactctc</b> gtgactggagttcagacgtgtgctcttccgatct	
28	caagcagaagacggcatacagagat <b>gtaacgac</b> gtgactggagttcagacgtgtgctcttccgatct	
29	caagcagaagacggcatacagagat <b>attcctcc</b> gtgactggagttcagacgtgtgctcttccgatct	
30	caagcagaagacggcatacagagat <b>gtgttcct</b> gtgactggagttcagacgtgtgctcttccgatct	
31	caagcagaagacggcatacagagat <b>aagcactg</b> gtgactggagttcagacgtgtgctcttccgatct	
32	caagcagaagacggcatacagagat <b>ctagcaag</b> gtgactggagttcagacgtgtgctcttccgatct	
33	caagcagaagacggcatacagagat <b>tgcttcca</b> gtgactggagttcagacgtgtgctcttccgatct	
34	caagcagaagacggcatacagagat <b>gcttagct</b> gtgactggagttcagacgtgtgctcttccgatct	
35	caagcagaagacggcatacagagat <b>aaccgttc</b> gtgactggagttcagacgtgtgctcttccgatct	
36	caagcagaagacggcatacagagat <b>gacattcc</b> gtgactggagttcagacgtgtgctcttccgatct	
37	caagcagaagacggcatacagagat <b>agaccgta</b> gtgactggagttcagacgtgtgctcttccgatct	
38	caagcagaagacggcatacagagat <b>gatactgg</b> gtgactggagttcagacgtgtgctcttccgatct	
39	caagcagaagacggcatacagagat <b>tgcttaga</b> gtgactggagttcagacgtgtgctcttccgatct	
40	caagcagaagacggcatacagagat <b>tcggttac</b> gtgactggagttcagacgtgtgctcttccgatct	
41	caagcagaagacggcatacagagat <b>atgacgtc</b> gtgactggagttcagacgtgtgctcttccgatct	
42	caagcagaagacggcatacagagat <b>gctgtaag</b> gtgactggagttcagacgtgtgctcttccgatct	
Primers for quantitative PCR		
Gene	Primer 1	Primer 2
<i>Jph2</i>	gtccaacatcgcccgtacatt	gccgacgcttctgatactcc
<i>Gapdh</i>	aggctcgggtgtgaacggatttg	tgtagaccatgtagttgaggtca
<i>Nppa</i>	ttcctcgtcttggccttttg	cctcatcttctaccggcatc
<i>Nppb</i>	gtccagcagagacctcaaaa	aggcagagtcagaaactgga
<i>Myh7</i>	gcgactcaaaaagaaggactttg	ggcttgctcatcctcaatcc
<i>AAV titer</i>	tcgggataaaaagcagtctgg	ccaagctattgtgtggcct

**Online Table III. Antibodies and dyes used in this study**

<b>Name</b>	<b>Dilution (Application)</b>	<b>Company</b>	<b>Cat. No.</b>
<i>Primary Antibodies</i>			
Rb-anti-JPH2	1:200 (IF), 1:2000 (WB)	Invitrogen	405300
Gt-anti-CAV3	1:200 (IF)	Santa Cruz	7665
Ms-anti-ACTN2	1:500 (IF)	Abcam	9465
Gt-anti-Troponin I	1:500 (IF)	Abcam	56357
Ms-anti-RYR2	1:200 (IF)	Abcam	2728
Gt-anti-NKX2-5	1:200 (IF)	Santa Cruz	8697
Ms-anti-TEAD1	1:500 (IF)	BD	610923
Rb-anti-BIN1	1:2000 (WB)	Rockland	200-301-E63
Rb-anti-GFP	1:5000 (WB)	GenScript	A01388-40
Rb-anti-GAPDH	1:5000 (WB)	Santa Cruz	25778
<i>Secondary Antibodies</i>			
555-Dk-anti-Gt	1:1000	Invitrogen	A21432
555-Dk-anti-Ms	1:1000	Invitrogen	A31570
555-Dk-anti-Rb	1:1000	Invitrogen	A31572
647-Dk-anti-Gt	1:1000	Invitrogen	A21447
647-Dk-anti-Ms	1:1000	Invitrogen	A31571
647-Dk-anti-Rb	1:1000	Invitrogen	A31573
HRP-Dk-anti-Rb	1:5000	Invitrogen	A16035
<i>Fluorescent Dyes</i>			
DAPI	500 nM	Invitrogen	D3571

555-WGA	5 µg/ml	Invitrogen	W32464
647-WGA	5 µg/ml	Invitrogen	W32466
FM 4-64	100 µg/ml	Invitrogen	T13320

---

## **E. Online Movies**

Online Movie I. *In situ* T-tubule imaging in a Jph2\_Low heart.

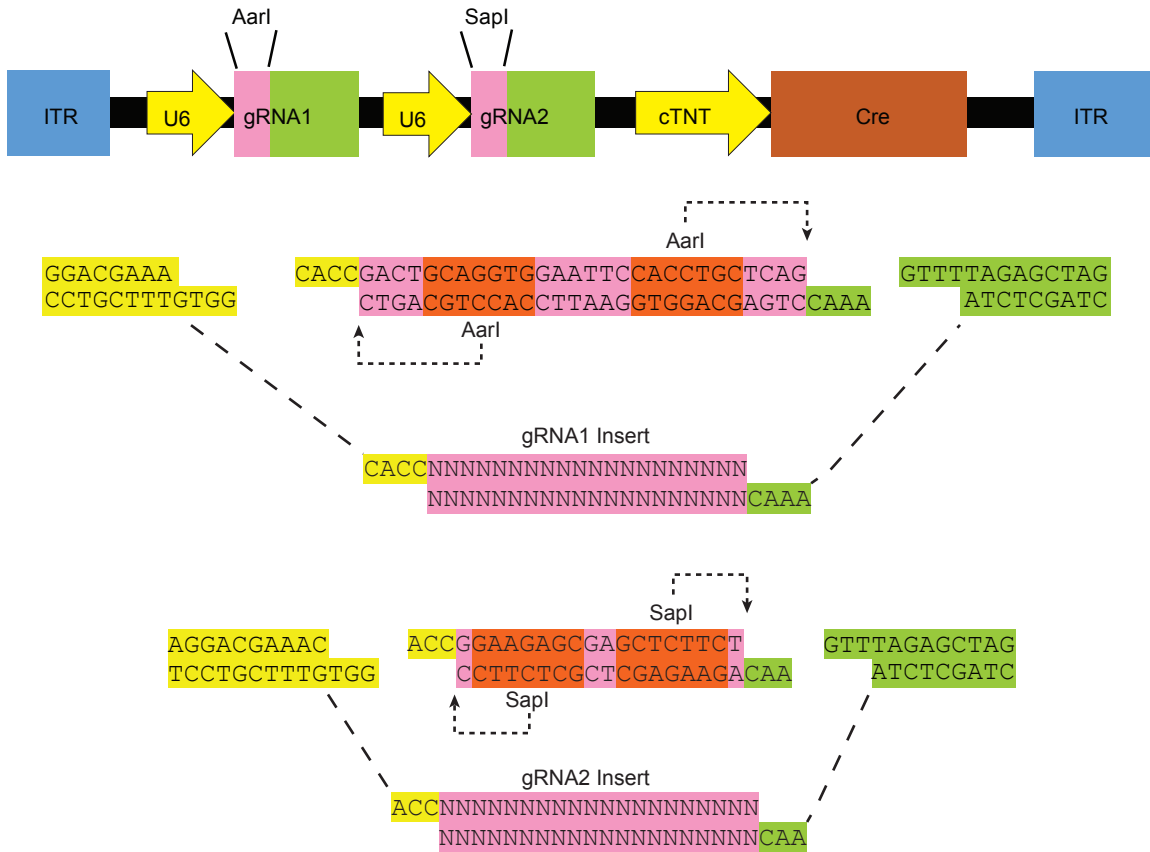
Online Movie II. *In situ* T-tubule imaging in a Jph2\_Mid heart.

Online Movie III. *In situ* T-tubule imaging in a Jph2\_High heart.

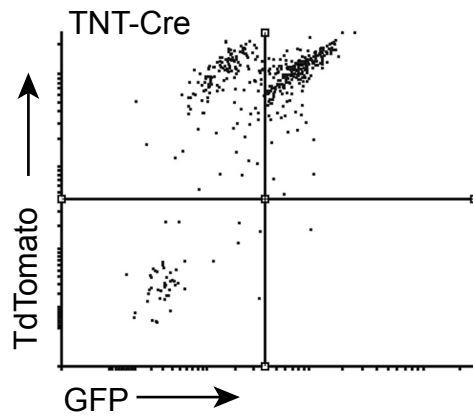
Online Movie IV. *In situ* T-tubule imaging in a RYR2 mosaic mutagenesis heart.

All movies are confocal z-stacks with 2  $\mu\text{m}$  step size that play at 1 stack/second speed. Each movie contains an FM4-64 grey-scale channel to the left and an RGB channel to the right that merges FM4-64 (Magenta) and Cas9GFP (Green) signals. The height of all movie frames is 212  $\mu\text{m}$ .

## D. Online Figures



**Online Figure I. AAV ITR vector for delivery of tandem guide RNAs and cTNT Cre.** The targeting sequences for gRNA1 and gRNA2 are inserted after AarI or SapI restriction digestion, respectively.



**Online Figure II. Distribution of GFP and tdTomato reporters in *Rosa26*<sup>Cas9GFP/tdTomato</sup> mice after treatment with AAV9:TNT-Cre.** Neonatal mice were treated with AAV:TNT-Cre. Cardiomyocytes were dissociated from adult hearts and analyzed by flow cytometry. As expected, most cardiomyocytes were GFP+ tdTomato+ and there were few GFP+ tdTomato- cells. However, GFP- tdTomato+ cells were noted. This might reflect differential sensitivity of the two different Cre-activated reporters to Cre, and differential sensitivity of GFP or tdTomato expression or stability in cardiomyocytes stressed by dissociation and flow cytometry.

**A**

The number of predicted off-target sites in mouse genome

Mismatch bp number	Jph2 gRNA1		Jph2 gRNA2	
	exonic	non-exonic	exonic	non-exonic
1	0	0	0	0
2	0	0	0	0
3	0	2	0	6

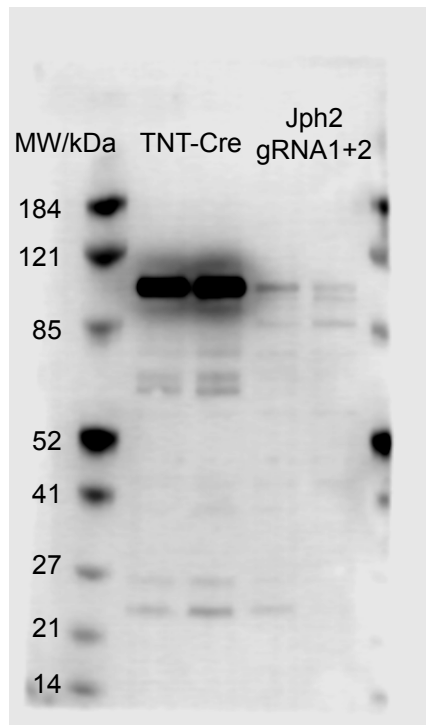
**B**

		gRNA1 target	PAM
Amp-Seq1 Jph2gRNA1	wildtype	GACTTTGATGATGGCGGGGCGTATTGTGG	GGGCTGGGAAGGGG
	frame-shift deletion	GACTTTGATGATGGCGGGGC-----TGGGAAGGGG	
	frame-shift insertion	GACTTTGATGATGGCGGGGCGTATTGTGGGGGCTGGGAAGGGG	

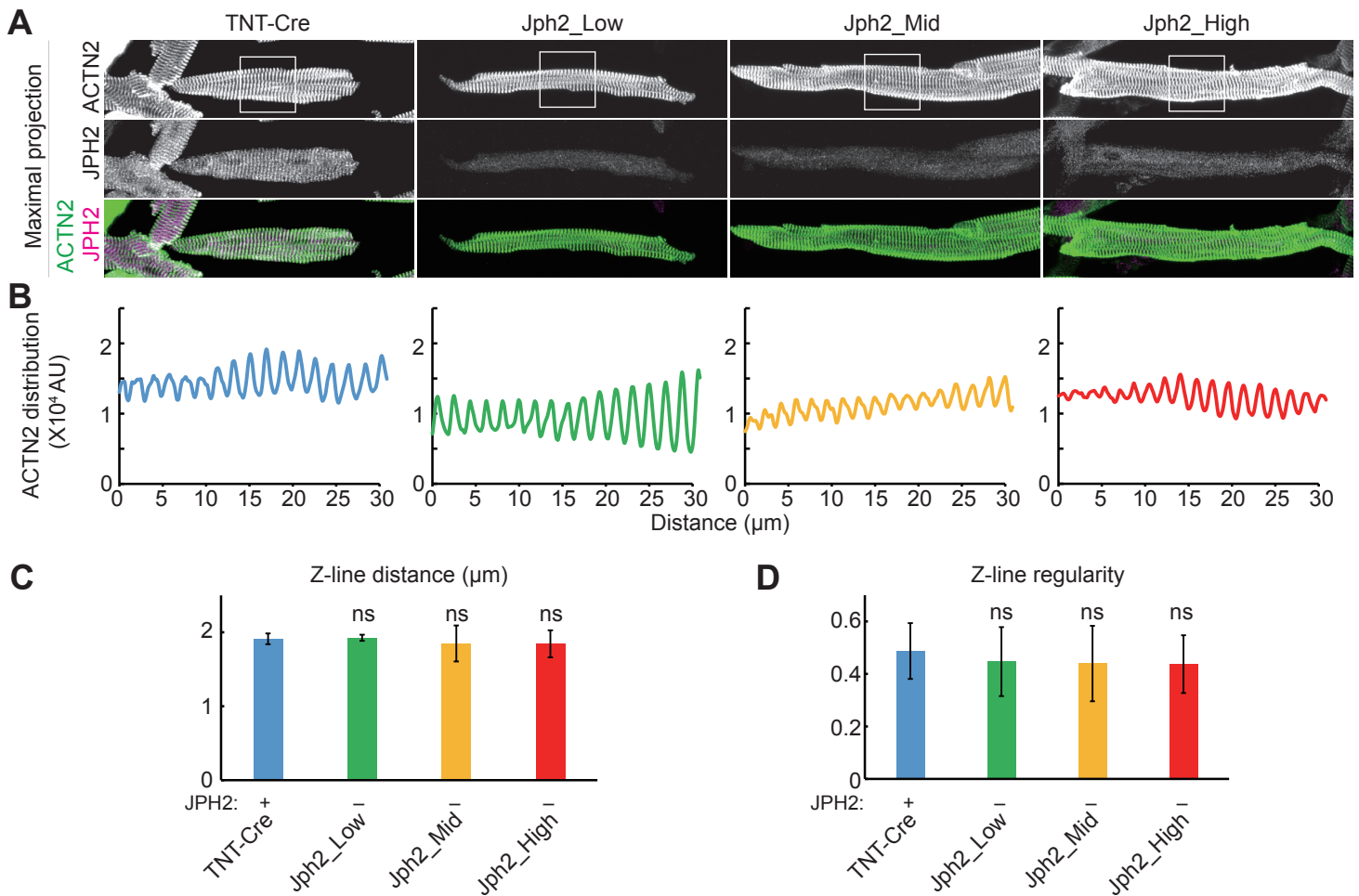
**C**

		PAM	gRNA2 target
Amp-Seq2 Jph2gRNA2	wildtype	CACAAACAGTGGTGCCAAGTACGAGGGCACTTGGAAAT	AACGGC
	frame-shift deletion	CACAAACAGTGGTGCCAAGT-----GGGCACTTGGAAAT	AACGGC
	frame-shift insertion	CACAAACAGTGGTGCCAAGTAACGAGGGCACTTGGAAAT	AACGGC

**Online Figure III. Frame-shift mutations induced by Jph2gRNA-directed Cas9 cleavage followed by NHEJ.** (A) The number of predicted off-target sites in the mouse genome for gRNA1 or gRNA2. (B-C) Examples of mutations induced by Jph2gRNA1 or Jph2gRNA2 as determined by amplicon sequencing.

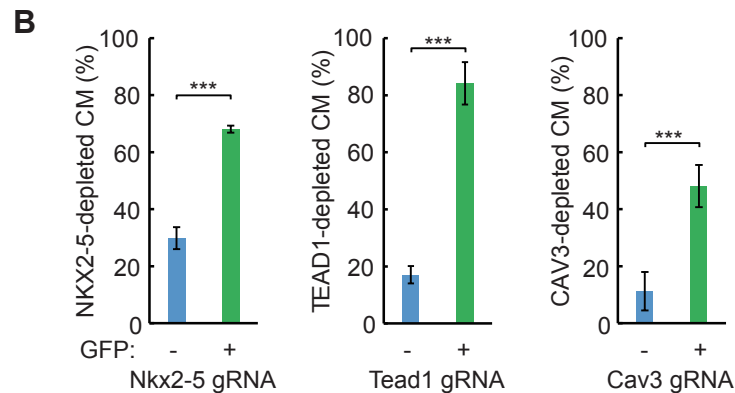
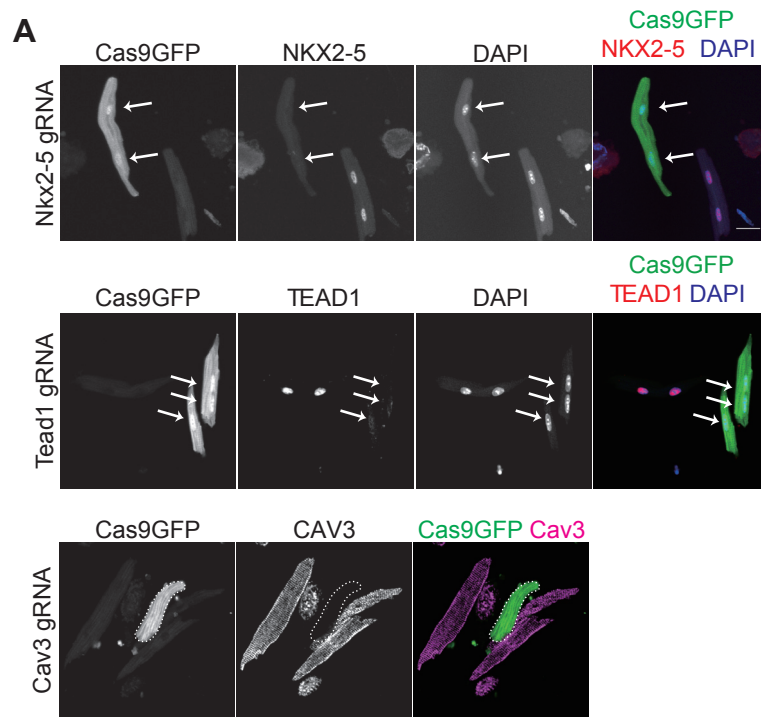


**Online Figure IV. JPH2 immunoblot of FACS-sorted GFP+ CMs treated with TNT-Cre or Jph2(gRNA1+2) AAV.** This is the full immunoblot of the same gel shown in Fig. 1G, over-exposed to look for minor truncated Jph2 expression products. The major effect of Jph2 gRNAs was reduction of JPH2 level rather than production of a truncated protein.

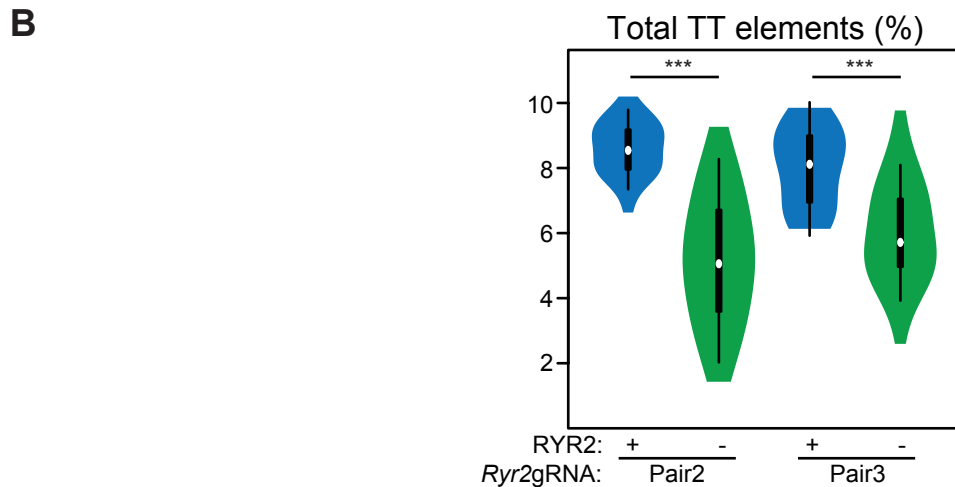
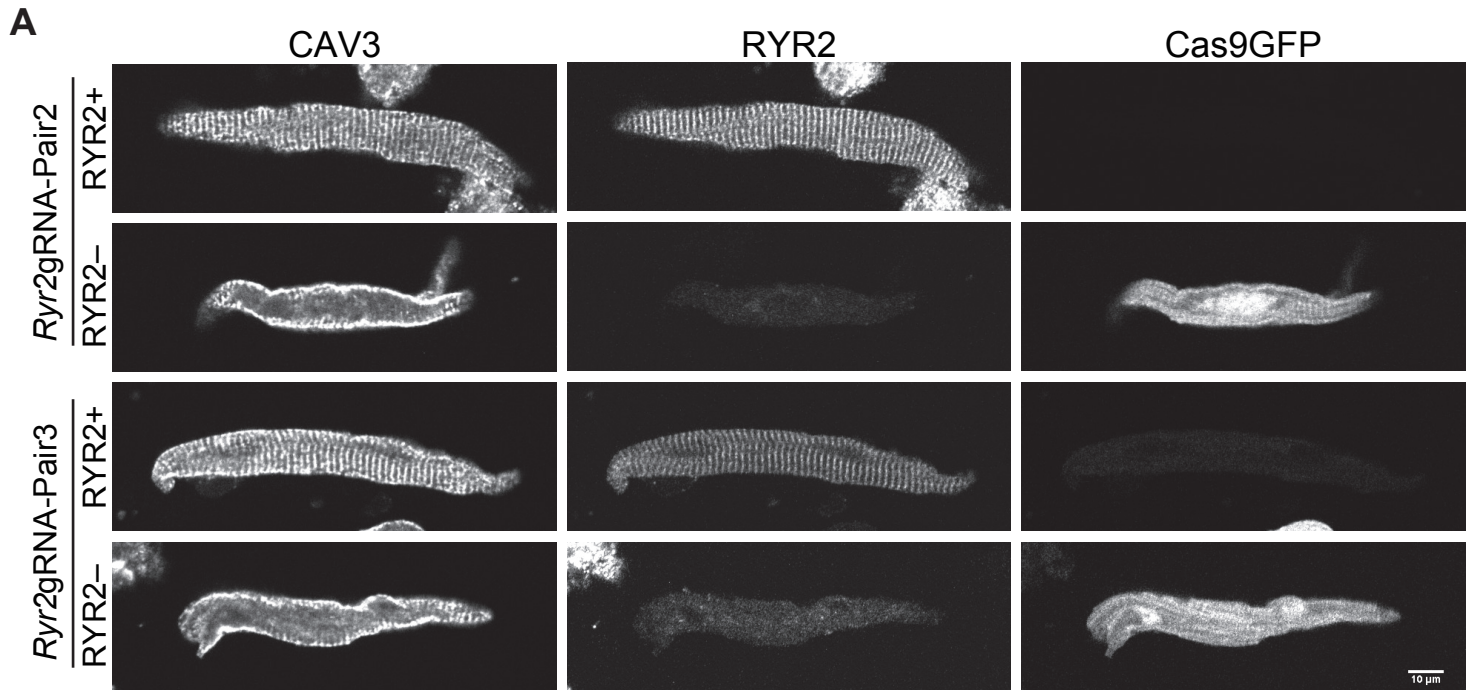


**Online Figure V. JPH2 depletion did not cell-autonomously disrupt sarcomere organization.**

TNT-Cre or AAV-gRNA(Jph2) were administered at P1 and CMs were isolated at P21. CMs were immunostained for JPH2 and ACTN2. (A) Representative maximal intensity projection images. (B) Longitudinal distribution of ACTN2 fluorescence intensity in a single focal plane of boxed areas in (A). AU, arbitrary unit. (C-D) Quantification of average distance between Z-lines and the regularity of Z-line alignment by AutoTT. Boxed areas in (A) were representative regions that were used to perform this quantification. n=30 CMs isolated from 3 hearts in each group. Student's t-test compared to control (TNT-Cre) cells. ns, not significant. Plots show mean  $\pm$  SD.



**Online Figure VI. Knockout of NKX2-5, TEAD1 and CAV3 by CASA AV.** (A) Immunofluorescence images showing depletion of NKX2-5 (top), TEAD1 (middle) and CAV3 (bottom) in Cas9GFP+ CMs upon mosaic transduction with AAVs that express corresponding gRNAs. Arrows point to nuclear depletion of NKX2-5 and TEAD1. CAV3-depleted cell is delineated by dashed lines. Scale bar, 20  $\mu$ m. (B) Quantification of NKX2-5, TEAD1 and CAV3 depletion in GFP- and GFP+ CMs. n=3 hearts. >50 CMs were counted per heart. Student's t-test: \*\*\*p<0.001. Plots show mean  $\pm$  SD.



**Online Figure VII. Mosaic RYR2 depletion using multiple gRNA pairs disrupts T-tubule structure.**

(A) RYR2 was depleted using two different pairs of gRNAs. RYR2 and CAV3 were detected by immunostaining, and GFP was detected by endogenous fluorescence. Representative images show that CAV3 T-tubule staining was disrupted by depletion of RYR2 in Cas9GFP+ CMs. Scale bar, 10 micron.

(B) Quantification of CAV3 immunostaining using AutoTT, displayed as violin plots. CMs depleted of RYR2 by either pair of gRNAs had reduced T-tubule organization. Student's t-test: \*\*\*,  $P < 0.001$ .